1 **Title**

2 **Stable twin rDNA loci form a single nucleolus in brewer's yeast**

3

4 **Authors**

5 Luciana Lazar-Stefanita[1], Jingchuan Luo[1†], Max A. B. Haase[1,2], Weimin Zhang[1], Jef D.

6 Boeke[1,3]*

7 *, Corresponding author: jef.boeke@nyulangone.org

8 **Affiliations**

9 [1] Institute for Systems Genetics and Department of Biochemistry and Molecular Pharmacology,

10 NYU Langone Health, New York, NY 10016, USA

11 [2] Vilcek Institute of Graduate Biomedical Sciences at NYU School of Medicine

12 [3] Department of Biomedical Engineering, NYU Tandon School of Engineering, Brooklyn NY

13 11201 USA

14 † Present address: Whitehead Institute for Biomedical Research, Cambridge, MA, 02142, USA

15

16 **Keywords**

17 Megablock chromosome engineering, Hi-C genome maps, intra-chromosomal rDNA loci,

18 nucleolar organization, liquid-liquid phase separation.

19

Abstract

The nucleolus is the most prominent membraneless compartment within the nucleus[1,2] - dedicated to the metabolism of ribosomal RNA. Nucleoli are composed of hundreds of ribosomal DNA (rDNA) repeated genes that form large chromosomal clusters[3–5], whose high recombination rates can cause nucleolar dysfunction and promote genome instability[6–8] related to metabolic and genetic diseases[9–13]. Intriguingly, the evolving architecture of genomes appears to have favored two strategic rDNA locations in a broad range of species – where a single locus per chromosome is situated either near the centromere or the telomere[14,15]. To delve into how organisms may benefit from these nuclear organizations, we used a fused-karyotype strain of *Saccharomyces cerevisiae*[16] to megabase-engineer a chromosome with twin chromosome-collinear rDNA loci. We showed that the twin-rDNA yeast readily adapts exhibiting wild-type growth and maintaining rRNA homeostasis. Using imaging and chromosome conformation capture, we found that the twin loci merge into a single subnuclear compartment throughout the cell cycle. Unexpectedly, we found that rDNA locus size is dependent on its position relative to the centromere, whereby the locus that is centromere–distal undergoes size reduction at a higher frequency compared to the centromere-proximal counterpart. In sum, our work sheds light on the structural evolution of rDNA loci and provides new tools to study the rDNA dosage effect on cellular metabolism.

38 **Introduction**

39 The most abundant genes in cells are those encoding ribosomal RNA (rRNA), usually arranged as
40 a series of tandem repeats that include transcriptional units for rRNAs spaced by non-transcribed
41 sequences[3,17]. As rRNAs are the structural components of ribosomes, they represent the most
42 abundant RNA molecules in most organisms, accounting for 60-70% of cellular transcripts e.g.,
43 10^5/yeast cell[18] and 10^{6-7}/animal cell[1].

44 In eukaryotes, rRNA transcription and ribosome assembly take place in a membraneless organelle
45 that occupies a substantial proportion of the cell nucleus, namely the nucleolus[2,19]. Ostensibly
46 incongruous features of the nucleolus – such as rapid molecular turnover and liquid-like dynamics,
47 yet maintaining a coherent shape – are reconciled by the liquid-liquid phase separation model[1,20],
48 which proposes that rRNA and associated proteins self-organize based on their intrinsic
49 biophysical properties[21]. Moreover, the structure and activity of the nucleolus are highly dynamic
50 throughout cell division, as is evident in eukaryotes with open mitosis in which nucleolar
51 breakdown and transcriptional shutdown are concomitant with entry into mitosis[22,23]. Nucleoli
52 assemble around distinct chromosomal clusters/loci, gathering hundreds of tandemly repeated
53 rDNA genes that largely exceed the number of units needed for survival. Indeed, typically, only
54 ~50% of the rDNA genes are actively transcribed while the remainder are kept inactive, an
55 equilibrium that can be readily tuned by altering the balance between euchromatin and
56 heterochromatin status at this locus[24,25]. Furthermore, a high rRNA level - positively correlated
57 with growth rate in many microbes[26] - can be achieved not only by boosting transcription but also
58 by rDNA copy number expansion[27]. Given their repetitive nature and the high demand for rRNA
59 transcripts, the rDNA loci are among the most unstable genome structures[7,28]. Their instability
60 relies on a repeat-mediated homologous recombination (HR) mechanism that requires both rDNA

61 replication[27,29] and transcriptional processes[30,31] that often result in clonal size variation in the
62 repeat number.
63 Cyto-taxonomic studies, based on the widespread usage of fluorescence in situ hybridization,
64 enabled mapping of rDNA loci on chromosomes of thousands of species. Number and position of
65 these loci, each containing hundreds of tandem repeats, were compiled and used for in silico
66 analyses of their evolution in plants[14] and animals[15]. To reveal that most taxa have genomes with
67 multiple rDNA loci, with an average number of only three to four loci per diploid genome,
68 indicating that most organisms tend to maintain a moderately low number of loci. In plants, locus
69 number was positively correlated with genome size; whereas in animals no such correlation was
70 observed. Surprisingly, although rDNA loci were identified at nearly any chromosomal position,
71 they prevalently appear either pericentromeric and/or peritelomeric (in >75% of karyotypes).
72 Genome-wide studies in mammals[32] and yeasts[33] provided evidence to support the hypothesis that
73 rDNA arrays have changed their chromosomal position multiple times during evolution: in almost
74 every case, the array disappeared entirely from the ancestral site, leaving behind a small 'intergenic
75 scar'[33].
76 These insights hint at two potential aspects of rDNA evolution: (*i*) a common ancestral mechanism
77 through which this locus may migrate within genomes and (*ii*) deleterious effects associated with
78 more than a single rDNA locus per chromosome. Regarding the first hypothesis, we can only
79 speculate that HR and 'nonreciprocal crossover' between repeats[34–36] may be responsible for
80 rDNA dynamics. Here we address the second hypothesis by monitoring the effects of a rDNA
81 migration event in which the entire native megabase rDNA array was transplanted to an ectopic
82 intra-chromosomal location through a copy-and-paste mechanism.
83

84 **Results**

85 In budding yeast, such as *Saccharomyces cerevisiae*, the *RDN1* locus is approximately 1.5 Mb
86 region that contains 150 – 200 copies of a 9.1 kb unit and accounts for ~10% of the entire yeast
87 genome[37]. Each repeat encodes four genes: 5.8S, 25S, 18S and 5S rRNAs transcribed by RNA
88 polymerase I and III[38,39]. The entire array exists in single copy on the right arm of chromosome
89 *12*, located roughly 300 kb from *CEN12* and ~600 kb from *TEL12R* [4,40], and forms a single crescent
90 shaped nucleolus apposed to the nuclear envelope[41] (Figure 1a). To assess whether multiple rDNA
91 loci can support yeast viability, previously constructed strains with a single locus on different
92 chromosomes (chr *12* and chr *3*)[42] were mated and the resulting diploid was sporulated. This
93 allowed the isolation of a haploid strain carrying two rDNA clusters on heterologous
94 chromosomes, validated through pulsed-field gel electrophoresis (PFGE) (Extended Data Figure
95 1a). Notably, this strain displays a single nucleolar compartment (Figure 1b; Extended Data Figure
96 1b). These results led us to conclude that yeast (just like many other eukaryotes) can readily adapt
97 to live with multiple rDNA loci on different chromosomes. However, it leaves unanswered the
98 question of whether the yeast genome can be engineered with multi-megabase rDNA loci
99 coexisting on the same chromosome.

100 *rDNA Megablock engineering: one step transplantation of a megabase locus to a target position*

101 To answer the above question, we used a karyotype-engineered yeast strain carrying three
102 megabase-sized chromosomes (*n*=3; with chromosomes *A*, *B* and *C*) that have been previously
103 generated through sequential telomere fusion events of the sixteen wild-type chromosomes[16].
104 These genome reengineering steps gave rise to megachromosome *C* (5.5 Mb-long), that resulted
105 in a dramatic change in the position of the rDNA locus relative to the nearest active centromere
106 (left drawing in Figure 1c, the black arrowhead points to the rDNA distal position). Precisely

107 stated, on chr *C,* the rDNA-centromere distance increased 9-fold relative to the wild-type distance,
108 reaching up to ~2.7 Mb, whereas its native position relative to the nearest (right arm) telomere
109 remained unchanged. Not only did this 'passive' migration of the locus to a distal location not
110 affect growth (see JL411 strain generated by Luo et al.[16]), but it also provided a chromosomal arm
111 long enough to allow for an insertion of a second centromere-proximal locus in *cis* (right drawing
112 in Figure 1c). Here we developed a variation of the CRISPR-Cas9 editing approach to engineer
113 megachromosomes that we call 'Megablock engineering' (Figure 1c; Methods), in which a
114 megabase-sized segment of a chromosome is moved to a target location, potentially anywhere in
115 the genome. Megablock engineering deploys two CRISPR guide RNAs that cut at the boundaries
116 of the genomic DNA 'block' to be relocated, and a third guide cutting at the target location.
117 Additionally, three 'linker DNAs' are provided: one that joins the native rDNA locus flanking
118 ends together, and two that join the left and right junctions of the target locus to the ends of the
119 megablock (Figure 1c). In this case, the entire megabase long rDNA locus was removed from its
120 native centromere-distal location and relocated 2 Mb closer to the chr *C* centromere. This
121 extremely aggressive genome engineering maneuver was surprisingly efficient, with 6/41 colonies
122 score by PCR genotyping showing evidence of successful megablock engineering. Hi-C was used
123 to structurally validate the rDNA locus transplantation (Figure 1d, black arrowheads point at the
124 rDNA boundaries). One such strain (JL665), with *CEN* proximal rDNA was then used for further
125 analyses and experiments. Of note, the orientation of the transplanted rDNA array relative to the
126 chromosome was maintained to ensure locus directionality (e.g., rDNA replication and
127 transcription orientation occur telomere-to-centromere in both the JL665 strain and its JL411
128 parent with *CEN* proximal or distal rDNA loci, respectively). By mating 'parental' and
129 'transplanted' strains, with either centromere-distal or centromere-proximal rDNA, respectively,

130 we generated a heterozygous diploid with two loci asymmetrically positioned on each homolog of
131 megachromosome *C*. Finally, haploids with duplicated rDNA loci in *cis* were isolated by
132 sporulation of this diploid strain and their integration junctions were PCR-verified (Extended Data
133 Figure 1c, d).

134 *Effects of rDNA duplication on fitness*

135 Whole genome sequencing validated the duplication of the rDNA locus in the haploid strains
136 (LS71 with 'twin' rDNA loci) by estimating twice as many rDNA-mapping reads in 2xrDNA/chr
137 *C* (Figure 2a). Importantly, the newly formed rDNA junction sequences were confirmed and no
138 chromosomal abnormalities potentially caused by recombination events between the two collinear
139 loci were detected (Extended Data Figure 2a). Not only did the 2xrDNA isolates lack obvious
140 fitness defects (Figure 2b; Extended Data Figure 2b), but they rapidly adapted to the excess of
141 rDNA repeats by fine-tuning the rRNA levels (Figure 2c; Extended Data Figure 2c). In addition,
142 a small number of genes were differentially expressed in the 2xrDNA vs. 1xrDNA strains (Figure
143 2d; Extended Data Table 2) and represented a nonrandom coherent set of genes. Notably, genes
144 involved in the metabolism of glucose and metal transport were downregulated, whereas phosphate
145 starvation-induced genes were upregulated. These results suggest that twin-rDNA cells may
146 experience a delayed metabolic transition from glucose fermentation (fast-growth) to respiration
147 (slow-growth) in response to nutrient deprivation.

148 Links between function and structure of the rDNA locus in yeast have been previously described,
149 and showed that a subset of the repeats are usually actively transcribed while the remainder are
150 silenced[25,43]. Their transcription level was correlated with distinct chromatin states, defined by the
151 association of the repeats with DNA-folding markers of either euchromatin (e.g., High-mobility
152 group proteins, Hmo1[44]) or heterochromatin (e.g., silencing complex, SIR[45]). Here we identified

153 mild changes in the expression level of these chromatin modifiers: the rDNA-silencing factor
154 (Sir2) was upregulated, whereas the active rDNA copy-associated protein Hmo1 was
155 downregulated in 2xrDNA compared to 1xrDNA strains (Extended Data Figure 2d). This
156 transcriptional anticorrelation is consistent with an excess of repeats in twin-rDNA strains that
157 may demand additional silencing.
158 Next, we investigated the structural organization of chr *C* with twin-rDNA loci in *cis,* and their
159 chromosomal (in)stability.
160 *Structure of chromosomes with twin-rDNA loci in cis*
161 We used Hi-C[46,47] to probe the 3-dimensional (3D) structure of genomes with twin-rDNA arrays.
162 The 2D contact maps of chr *C* containing a single locus, either centromere-proximal or distal, were
163 combined in a single control plot. For comparison purposes, the control plot is displayed adjacent
164 to that obtained from strains with *cis* twin-rDNA loci (Figure 3a). In the control plot, two
165 indistinguishable boundaries formed at each rDNA location, as a result of similar insulation rates
166 from their corresponding adjacent regions. In contrast, the two boundaries in *cis* appeared to give
167 rise to distinct contact frequencies, where the insulation ('sharpness') at the *CEN* proximal rDNA
168 cluster prevailed over the distal twin. This observation was validated through contact
169 quantification plots for each locus that considered contacts between the intervening region
170 enclosed by the two loci and the corresponding non-intervening rDNA-flanking regions
171 (highlighted by blue dashed rectangles in Figure 3a). From this analysis we observed that the distal
172 locus forms a weaker chromosome boundary (lower degree of insulation) when its centromere-
173 proximal twin is located in *cis* (Figure 3b), a result that suggested distinct levels of structural
174 'bulkiness' between the *cis* rDNA loci.

175 Given that the 2xrDNA map represents consistent results obtained from 3 independent yeast
176 isolates, we reasoned that the structural difference between the twin loci may arise from distinct
177 epigenetic or genetic effects. Two major chromatin modifications at the distal locus could
178 potentially be responsible for this divergence: (*i*) increased heterochromatin that may result in a
179 highly condensed/compacted structure, and/or (*ii*) a reduction of rDNA repeat copy number. As
180 the two loci are identical in sequence, we were unable to distinguish between rRNA transcripts
181 originating from either locus (see discussion). Even though we may be unable to rule out the
182 hypothesis of different levels of heterochromatin at the two *cis* rDNAs, their overall lengths can
183 be directly measured. The size of each rDNA locus was estimated using PFGE and dual color
184 Southern blotting on BamHI-digested chromosomes (Figure 3c, d; Methods). After digestion with
185 BamHI, which does not cut within the rDNA repeat unit, the rDNA loci were left with unique
186 DNA-flanking sequences, utilized to design probes that specifically recognize each locus.
187 Surprisingly, all 2xrDNA isolates showed a consistent and locus-specific size reduction of the
188 distal rDNA locus of ~500-700 kb when compared to the 1xrDNA-distal parent strain (Figure 3d;
189 Extended Data Figure 3a, b). Also, a higher clonal variability in the size of the distal locus was
190 observed in isolates passaged for ~100 generations (Extended Data Figure 3c). These results led
191 us to hypothesize that rDNA repeats in yeast are more stable when located centromere-proximal
192 rather than distal. To our knowledge this is the first evidence of a direct correlation between size
193 of a repeated region and its relative genome location.
194 Finally, we probed the stability of the two loci in *cis* in function of Sir2, known to suppress
195 recombination between repeated ribosomal genes[30,45]. We found that the two distinct rDNA bands
196 were lost (replaced by DNA smear) in all Δ*sir2* isolates (Extended Data Figure 3d), supporting the
197 idea that the specific size variation of the two loci in *cis* may depend on differential Sir2 activity.

198 *Mitotic reorganization of the nucleolus with cis rDNAs*

199 For the nucleolus to be correctly segregated between mother and daughter cells in late anaphase,
200 rRNA transcription needs to be shut down to achieve rDNA-cluster condensation[48,49]. Importantly,
201 these condensation processes mainly involve the rDNA and are less pronounced across the
202 remainder of the yeast genome.

203 Our previous work showed that the mitotic reorganization of chromatin is preserved along mega-
204 chromosomes (Lazar-Stefanita et al., 2022 in press). Here, we specifically addressed the structure
205 of megachromosome *C* with twin *cis* rDNAs and that of the resulting nucleolus during the cell
206 cycle. Overall we expected chr *C* to undergo a typical mitotic reorganization[50], however it
207 remained unknown how the ~1.9 Mb-long non-rDNA sequence linking the two loci may interfere
208 with the structure of the nucleolus. Cells synchronized in G1 (alpha-factor) and in anaphase
209 (*cdc15-2* ts[51]) were imaged and showed very clearly that the two rDNAs consistently formed a
210 single nucleolar mass per cell throughout mitosis (Figure 4a; Extended Data Figure 4a).

211 The Hi-C maps revealed yet another layer of structural complexity of the nucleolus. The G1 map
212 displayed strong contacts between the two rDNAs in *cis*, but these were lost in late anaphase
213 (Figure 4b, black arrowhead; Extended Data Figure 4c). Contact quantifications between the
214 rDNA-flanking regions (as described in Figure 3a, b) showed an overall decrease in anaphase
215 compared to G1 (Figure 4b), in agreement with their increased condensation during anaphase that
216 may strengthen chromosome boundaries. Note that the folding status of the rDNA-intervening
217 sequence on chr *C* is not influenced by the rDNA-flanking loci (Extended Data Figure 4b, contact
218 probability $p(s)$ decay). Therefore, we conclude that (*i*) the ~1.9 Mb rDNA-intervening sequence
219 does not interfere with the organization of the nucleolus, and that (*ii*) the two loci are treated as
220 distinct chromosomal entities during anaphase condensation.

221 **Conclusion and discussion**

222 Here we provided the first living evidence of a eukaryotic genome carrying more than one rDNA
223 locus located within the same chromosomal arm. The remarkable stability of the yeast genome is
224 highlighted in its transcriptomics and the homeostatic control of the rDNA repeats at each locus.
225 The structure of the twin-rDNA nucleolus and its reorganization during cell cycle was investigated
226 using microscopy, showing a high degree of structural conformity between 1xrDNA and 2xrDNA
227 strains.

228

229 *Design of the strains*

230 Prior works on rDNA have employed interspecies hybrids to address if any differential stability of
231 this locus in different yeasts[52–54]. Most of these studies observed a uniparental loss of rDNA genes,
232 a relevant example is the hybrid between *S. cerevisiae* and *S. eubayanus* in which the latter's locus
233 collapsed completely whereas the *S. cerevisiae* remains full sized. Therefore, we reasoned that
234 only by using two native and sequence-identical rDNA arrays located at different positions along
235 the chromosome we could truly evaluate the position-effect on their structure and stability.

236 The ectopic location for rDNA mega-transplantation corresponds to a chromosome fusion site,
237 specifically the right and left ends of chr *15* and chr *4*, respectively. Given that these regions were
238 initially subtelomeric, which typically lack essential genes, we reasoned that they would be
239 'insensitive-to-insertion' sites for the huge rDNA locus. Finally, the two loci in *cis* conserved the
240 wild-type transcriptional orientation (telomere-to-centromere). Our results show a consistent
241 reduction in size of the centromere distal locus compared to the proximal counterpart. This peculiar
242 size readjustment appears to be Sir2-dependent (Extended Data Figure 3d) suggesting that the
243 transcriptional activity at the two loci maybe different. We speculate that the centromere-distal

244 locus, which is flanked by its native sequence, is predominantly transcribed and therefore more
245 prone to rapid size adjustments. Thus, explaining the homeostasis in rRNA level we observed.
246
247 *Nucleolus as a liquid condensate*
248 We found that the yeast rDNA readily forms a single nucleolus, independent of its: position in the
249 genome (homologous or heterologous chromosomes), number of loci per chromosome (single or
250 duplicated) and repeat size. This is in full agreement with the proposed liquid-liquid phase
251 separation model for the nucleolus[1,21], which envisions the intrinsic biochemical properties of the
252 rDNA as major driving forces for nucleolar assembly that can act over very long genomic
253 distances.
254
255 *Potential consequences of a twin-collinear organization of the rDNA loci*
256 Evolutionary analyses of rDNA loci suggested that selective pressure may act to preserve specific
257 characteristics (such as structure, number, and position) of these highly repeated loci in eukaryotes.
258 Here we found that placing two rDNA loci in *cis* increases the rate of abnormal meiotic
259 recombination (Extended Data Figure 5), possibly due to mispairing of the homologous
260 chromosomes driven by the rDNA loci. We speculate that the misaligned chromatids can undergo
261 unequal crossing-over resulting in an increased frequency of nonreciprocal exchange of genetic
262 information (or gene conversion) and concomitant spore lethality. Our current model suggests that
263 a high meiotic fitness cost is associated with multi-collinear repeated loci, and this would be
264 predicted to ultimately be purged from a sexual population.
265 In addition, the extra copy of the rDNA locus appears to affect the metabolic response to nutrient
266 consumption that would normally induce cells to exit the fast-growing phase, enter slow-growth

267 and eventually arrest. Our transcriptomics data seem to suggest that the rDNA surplus triggers a
268 premature response to starvation congruent with an apparently faster metabolism. Therefore, we
269 speculate that selective pressure acts to maintain rDNA repeat number within an effective 'optimal
270 range' that ensures rRNA levels can be readily tuned in response to environmental changes. More
271 generally, we term this potential fitness defect 'paralogous *cis*-rDNA interference', whereby
272 placement of two repeated and identical sequences in *cis* may cause interference with their function
273 and ultimately lead to the loss of one locus.
274 These findings are noteworthy in the context of rDNA expansions observed in tumor cells, which
275 are usually characterized by genome instability and rapid growth-associated metabolic states
276 predominantly based on fast glucose uptake and fermentation (e.g., the Warburg effect).

277 **Main references**

278 1. Lafontaine, D. L. J., Riback, J. A., Bascetin, R. & Brangwynne, C. P. The nucleolus as a
279 multiphase liquid condensate. *Nat. Rev. Mol. Cell Biol.* **22**, 165–182 (2021).
280 2. Thiry, M. & Lafontaine, D. L. J. Birth of a nucleolus: the evolution of nucleolar
281 compartments. *Trends Cell Biol.* **15**, 194–199 (2005).
282 3. Long, E. O. & Dawid, I. B. Repeated Genes in Eukaryotes. *Annu. Rev. Biochem.* **49**, 727–
283 764 (1980).
284 4. Petes, T. D. Yeast ribosomal DNA genes are located on chromosome XII. *Proc. Natl. Acad.*
285 *Sci. U. S. A.* **76**, 410–414 (1979).
286 5. Sylvester, J. E. *et al.* The human ribosomal RNA genes: structure and organization of the
287 complete repeating unit. *Hum. Genet.* **73**, 193–198 (1986).
288 6. Saka, K., Takahashi, A., Sasaki, M. & Kobayashi, T. More than 10% of yeast genes are
289 related to genome stability and influence cellular senescence via rDNA maintenance. *Nucleic*
290 *Acids Res.* **44**, 4211–4221 (2016).
291 7. Salim, D. & Gerton, J. L. Ribosomal DNA instability and genome adaptability. *Chromosome*
292 *Res.* **27**, 73–87 (2019).
293 8. Weeks, S. E., Metge, B. J. & Samant, R. S. The nucleolus: a central response hub for the
294 stressors that drive cancer progression. *Cell. Mol. Life Sci.* **76**, 4511–4524 (2019).
295 9. Ding, Q., Markesbery, W. R., Cecarini, V. & Keller, J. N. Decreased RNA, and Increased
296 RNA Oxidation, in Ribosomes from Early Alzheimer's Disease. *Neurochem. Res.* **31**, 705–
297 710 (2006).
298 10. Sönmez, A. *et al.* Nucleolar stress controls mutant Huntington toxicity and monitors
299 Huntington's disease progression. *Cell Death Dis.* **12**, 1–12 (2021).

300 11. Ganley, A. R. D. & Kobayashi, T. Ribosomal DNA and cellular senescence: new evidence
301 supporting the connection between rDNA and aging. *FEMS Yeast Res.* **14**, 49–59 (2014).
302 12. Sinclair, D. A., Mills, K. & Guarente, L. Accelerated Aging and Nucleolar Fragmentation in
303 Yeast sgs1 Mutants. *Science* **277**, 1313–1316 (1997).
304 13. Tiku, V. & Antebi, A. Nucleolar Function in Lifespan Regulation. *Trends Cell Biol.* **28**, 662–
305 672 (2018).
306 14. Garcia, S., Kovařík, A., Leitch, A. R. & Garnatje, T. Cytogenetic features of rRNA genes
307 across land plants: analysis of the Plant rDNA database. *Plant J.* **89**, 1020–1030 (2017).
308 15. Sochorová, J., Garcia, S., Gálvez, F., Symonová, R. & Kovařík, A. Evolutionary trends in
309 animal ribosomal DNA loci: introduction to a new online database. *Chromosoma* **127**, 141–
310 150 (2018).
311 16. Luo, J., Sun, X., Cormack, B. P. & Boeke, J. D. Karyotype engineering by chromosome
312 fusion leads to reproductive isolation in yeast. *Nature* **560**, 392–396 (2018).
313 17. Schöfer, C. & Weipoltshammer, K. Nucleolus and chromatin. *Histochem. Cell Biol.* **150**,
314 209–225 (2018).
315 18. Warner, J. R. The economics of ribosome biosynthesis in yeast. *Trends Biochem. Sci.* **24**,
316 437–440 (1999).
317 19. Pederson, T. The Nucleolus. *Cold Spring Harb. Perspect. Biol.* **3**, a000638 (2011).
318 20. Hansen, J. C., Maeshima, K. & Hendzel, M. J. The solid and liquid states of chromatin.
319 *Epigenetics Chromatin* **14**, 50 (2021).
320 21. Feric, M. *et al.* Coexisting Liquid Phases Underlie Nucleolar Subcompartments. *Cell* **165**,
321 1686–1697 (2016).

322 22. Boisvert, F.-M., van Koningsbruggen, S., Navascués, J. & Lamond, A. I. The multifunctional
323 nucleolus. *Nat. Rev. Mol. Cell Biol.* **8**, 574–585 (2007).
324 23. Hernandez-Verdun, D. Assembly and disassembly of the nucleolus during the cell cycle.
325 *Nucl. Austin Tex* **2**, 189–194 (2011).
326 24. Mekhail, K. & Moazed, D. The nuclear envelope in genome organization, expression and
327 stability. *Nat. Rev. Mol. Cell Biol.* **11**, 317–328 (2010).
328 25. Srivastava, R., Srivastava, R. & Ahn, S. H. The Epigenetic Pathways to Ribosomal DNA
329 Silencing. *Microbiol. Mol. Biol. Rev. MMBR* **80**, 545–563 (2016).
330 26. Weider, L. J. *et al.* The Functional Significance of Ribosomal (r)DNA Variation: Impacts on
331 the Evolutionary Ecology of Organisms. *Annu. Rev. Ecol. Evol. Syst.* **36**, 219–242 (2005).
332 27. Kobayashi, T., Heck, D. J., Nomura, M. & Horiuchi, T. Expansion and contraction of
333 ribosomal DNA repeats in Saccharomyces cerevisiae: requirement of replication fork
334 blocking (Fob1) protein and the role of RNA polymerase I. *Genes Dev.* **12**, 3821–3830
335 (1998).
336 28. Kobayashi, T. & Sasaki, M. Ribosomal DNA stability is supported by many 'buffer genes'—
337 introduction to the Yeast rDNA Stability Database. *FEMS Yeast Res.* **17**, fox001 (2017).
338 29. Sanchez, J. C. *et al.* Defective replication initiation results in locus specific chromosome
339 breakage and a ribosomal RNA deficiency in yeast. *PLoS Genet.* **13**, (2017).
340 30. Gottlieb, S. & Esposito, R. E. A new role for a yeast transcriptional silencer gene, SIR2, in
341 regulation of recombination in ribosomal DNA. *Cell* **56**, 771–776 (1989).
342 31. Kobayashi, T. & Ganley, A. R. D. Recombination Regulation by Transcription-Induced
343 Cohesin Dissociation in rDNA Repeats. *Science* **309**, 1581–1584 (2005).

344 32. Robicheau, B. M., Susko, E., Harrigan, A. M. & Snyder, M. Ribosomal RNA Genes
345 Contribute to the Formation of Pseudogenes and Junk DNA in the Human Genome. *Genome*
346 *Biol. Evol.* **9**, 380–397 (2017).
347 33. Proux-Wéra, E., Byrne, K. P. & Wolfe, K. H. Evolutionary Mobility of the Ribosomal DNA
348 Array in Yeasts. *Genome Biol. Evol.* **5**, 525–531 (2013).
349 34. Brown, D. D., Wensink, P. C. & Jordan, E. A comparison of the ribosomal DNA's of
350 Xenopus laevis and Xenopus mulleri: the evolution of tandem genes. *J. Mol. Biol.* **63**, 57–73
351 (1972).
352 35. Eickbush, T. H. & Eickbush, D. G. Finely Orchestrated Movements: Evolution of the
353 Ribosomal RNA Genes. *Genetics* **175**, 477–485 (2007).
354 36. Gibbons, J. G., Branco, A. T., Godinho, S. A., Yu, S. & Lemos, B. Concerted copy number
355 variation balances ribosomal DNA dosage in human and mouse genomes. *Proc. Natl. Acad.*
356 *Sci.* **112**, 2485–2490 (2015).
357 37. Petes, T. D. & Botstein, D. Simple Mendelian inheritance of the reiterated ribosomal DNA of
358 yeast. *Proc. Natl. Acad. Sci.* **74**, 5091–5095 (1977).
359 38. French, S. L., Osheim, Y. N., Cioci, F., Nomura, M. & Beyer, A. L. In Exponentially
360 Growing Saccharomyces cerevisiae Cells, rRNA Synthesis Is Determined by the Summed
361 RNA Polymerase I Loading Rate Rather than by the Number of Active Genes. *Mol. Cell.*
362 *Biol.* **23**, 1558–1568 (2003).
363 39. Nomura, M., Nogi, Y. & Oakes, M. *Transcription of rDNA in the Yeast Saccharomyces*
364 *cerevisiae*. *Madame Curie Bioscience Database [Internet]* (Landes Bioscience, 2013).
365 40. Kim, Y.-H. *et al.* Chromosome XII context is important for rDNA function in yeast. *Nucleic*
366 *Acids Res.* **34**, 2914–2924 (2006).

367 41. Dvorkin, N., Clark, M. W. & Hamkalo, B. A. Ultrastructural localization of nucleic acid
368 sequences in Saccharomyces cerevisiae nucleoli. *Chromosoma* **100**, 519–523 (1991).
369 42. Zhang, W. *et al.* Engineering the ribosomal DNA in a megabase synthetic chromosome.
370 *Science* **355**, (2017).
371 43. Smith, J. S. & Boeke, J. D. An unusual form of transcriptional silencing in yeast ribosomal
372 DNA. *Genes Dev.* **11**, 241–254 (1997).
373 44. Merz, K. *et al.* Actively transcribed rRNA genes in S. cerevisiae are organized in a
374 specialized chromatin associated with the high-mobility group protein Hmo1 and are largely
375 devoid of histone molecules. *Genes Dev.* **22**, 1190–1204 (2008).
376 45. Kobayashi, T., Horiuchi, T., Tongaonkar, P., Vu, L. & Nomura, M. SIR2 regulates
377 recombination between different rDNA repeats, but not recombination within individual
378 rRNA genes in yeast. *Cell* **117**, 441–453 (2004).
379 46. Dekker, J., Rippe, K., Dekker, M. & Kleckner, N. Capturing chromosome conformation.
380 *Science* **295**, 1306–1311 (2002).
381 47. Lieberman-Aiden, E. *et al.* Comprehensive mapping of long-range interactions reveals
382 folding principles of the human genome. *Science* **326**, 289–293 (2009).
383 48. Amon, A. A decade of Cdc14 – a personal perspective. *FEBS J.* **275**, 5774–5784 (2008).
384 49. Clemente-Blanco, A. Nucleolar Condensation: A New Mechanism to Control Mitotic Exit.
385 *Curr. Biol.* **27**, R1220–R1222 (2017).
386 50. Lazar-Stefanita, L. *et al.* Cohesins and condensins orchestrate the 4D dynamics of yeast
387 chromosomes during the cell cycle. *EMBO J.* **36**, 2684–2697 (2017).
388 51. Hartwell, L. H., Culotti, J., Pringle, J. R. & Reid, B. J. Genetic control of the cell division
389 cycle in yeast. *Science* **183**, 46–51 (1974).

390 52. Gordon, J. L. & Wolfe, K. H. Recent allopolyploid origin of Zygosaccharomyces rouxii
391 strain ATCC 42981. *Yeast* **25**, 449–456 (2008).
392 53. Louis, V. L. *et al.* Pichia sorbitophila, an Interspecies Yeast Hybrid, Reveals Early Steps of
393 Genome Resolution After Polyploidization. *G3 Bethesda Md* **2**, 299–311 (2012).
394 54. Nakao, Y. *et al.* Genome sequence of the lager brewing yeast, an interspecies hybrid. *DNA*
395 *Res. Int. J. Rapid Publ. Rep. Genes Genomes* **16**, 115–129 (2009).
396 55. Brachmann, C. B. *et al.* Designer deletion strains derived from Saccharomyces cerevisiae
397 S288C: a useful set of strains and plasmids for PCR-mediated gene disruption and other
398 applications. *Yeast Chichester Engl.* **14**, 115–132 (1998).
399 56. Zavala, A. G., Kulkarni, A. S. & Fortunato, E. A. A Dual Color Southern Blot to Visualize
400 Two Genomes or Genic Regions Simultaneously. *J. Virol. Methods* **198**, 64–68 (2014).
401 57. Truong, D. M. & Boeke, J. D. Resetting the yeast epigenome with human nucleosomes. *Cell*
402 **171**, 1508-1519.e13 (2017).
403 58. Bolger, A. M., Lohse, M. & Usadel, B. Trimmomatic: a flexible trimmer for Illumina
404 sequence data. *Bioinformatics* **30**, 2114–2120 (2014).
405 59. Bray, N. L., Pimentel, H., Melsted, P. & Pachter, L. Near-optimal probabilistic RNA-seq
406 quantification. *Nat. Biotechnol.* **34**, 525–527 (2016).
407 60. Engel, S. R. *et al.* The reference genome sequence of Saccharomyces cerevisiae: then and
408 now. *G3 Bethesda Md* **4**, 389–398 (2014).
409 61. Pimentel, H., Bray, N. L., Puente, S., Melsted, P. & Pachter, L. Differential analysis of RNA-
410 seq incorporating quantification uncertainty. *Nat. Methods* **14**, 687–690 (2017).
411 62. Schneider, C. A., Rasband, W. S. & Eliceiri, K. W. NIH Image to ImageJ: 25 years of image
412 analysis. *Nat. Methods* **9**, 671–675 (2012).

413 63. Langmead, B. & Salzberg, S. L. Fast gapped-read alignment with Bowtie 2. *Nat. Methods* **9**,
414 357–359 (2012).
415 64. Cournac, A., Marie-Nelly, H., Marbouty, M., Koszul, R. & Mozziconacci, J. Normalization
416 of a chromosomal contact map. *BMC Genomics* **13**, 436 (2012).
417

418 **Figures and figure legends**

419 **Figure 1 Transplantation of the rDNA megablock to ectopic genome locations.**

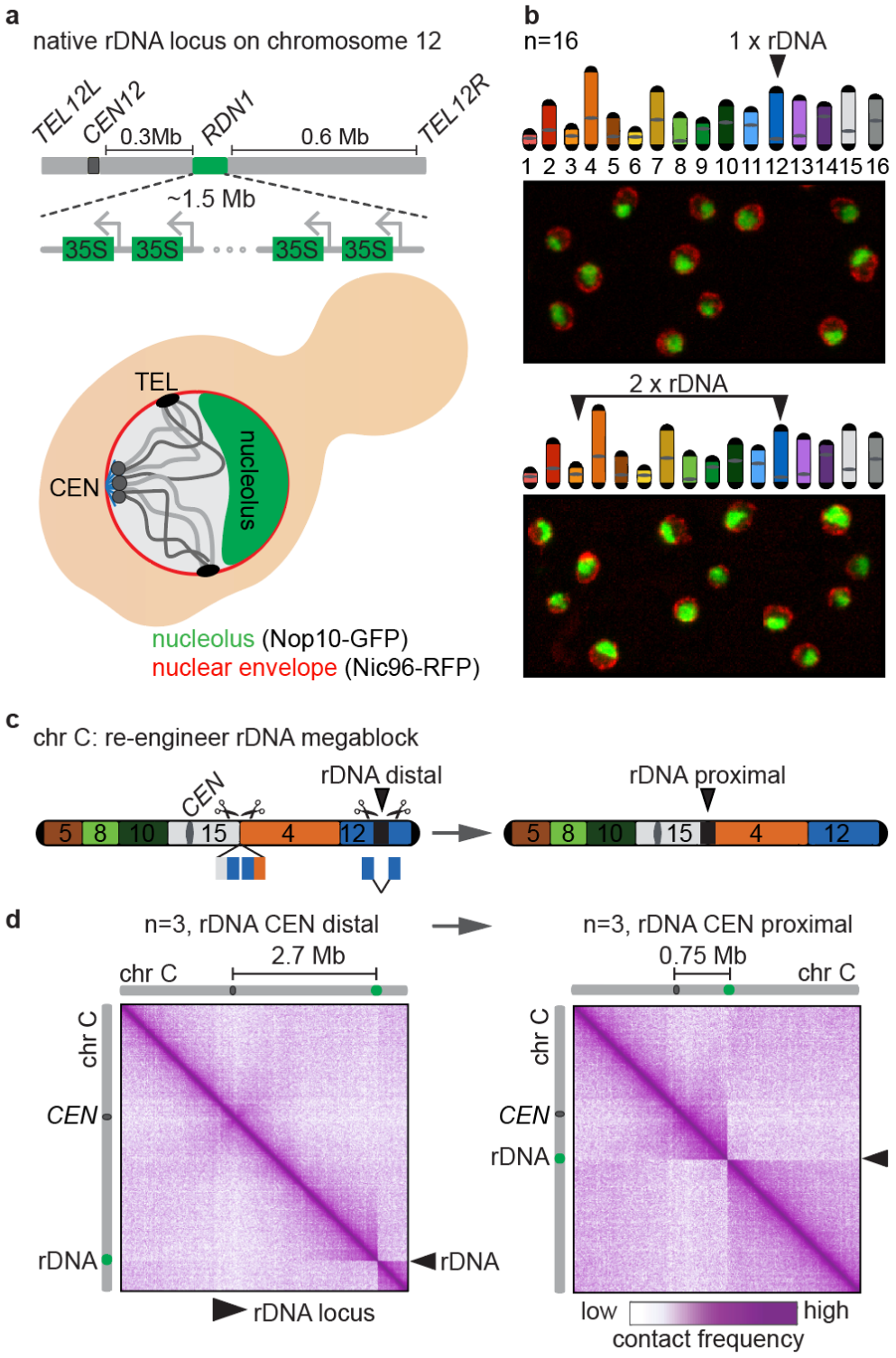

420

421 **Figure 1 Transplantation of the rDNA megablock to ectopic genome locations.**

422 **a** Diagram showing wild-type chromosome *12* that contains the rDNA locus (green) and a
423 simplified representation of nuclear organization in the wild-type yeast, where examples of
424 chromosome arms (gray lines) are anchored at the nuclear membrane through centromeres (*CEN*)
425 and telomeres (*TEL*). **b** Representative microscopy images of yeast nuclei with one or two rDNA
426 loci (black arrowheads in the schematic indicate rDNA containing chromosomes). **c** Schema
427 illustrating the relocation (arrowheads) of the rDNA megablock (black box) on the fused
428 megachromosome *C* (chr *C*: color code corresponds to the design of chromosome fusion) in yeasts
429 with *n*=3 chromosomes. Colored blocks indicate sequence homology of the repair donors at
430 CRISPR-Cas9 cutting sites. **d** Hi-C contact maps of chr *C* shown in gray on the *x*- and *y*-axis of
431 each map. The rDNA locus is *CEN* distal on the left, whereas, after transplantation it appears *CEN*
432 proximal on the right. rDNA distance from the centromere (dark gray) is indicated atop the maps.

433 **Figure 2 Effects of rDNA duplication on cell fitness.**

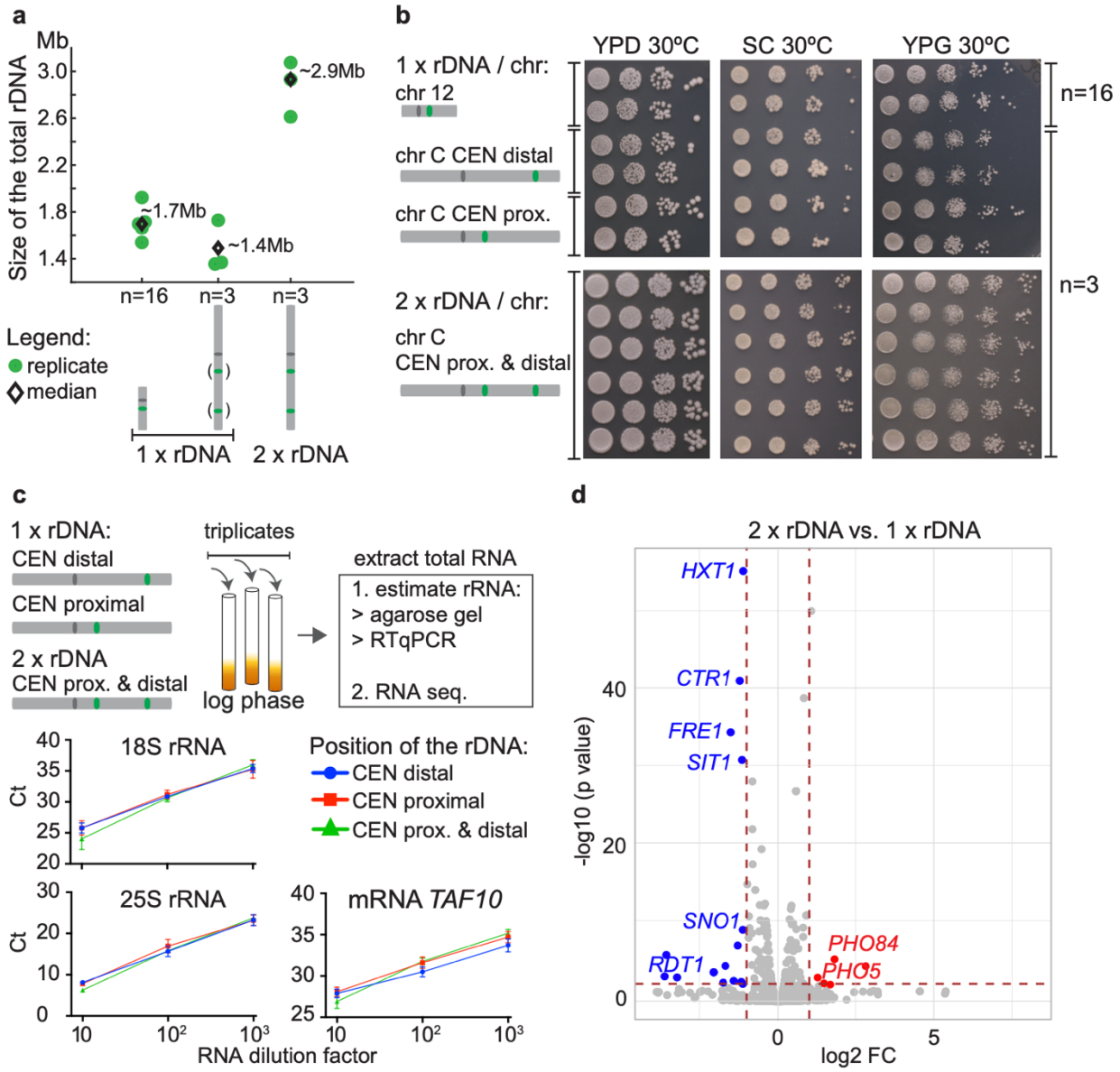

434

435 **Figure 2 Effects of rDNA duplication on cell fitness.**

436 **a** Estimate the total length of the rDNA by deep sequencing: % of rDNA aligned reads normalized
437 by genome size (12.3 Mb). Megachromosome *C* schematics are shown on the bottom of the plot
438 (gray), where round brackets indicate either the proximal or the distal rDNA locus (green). **b** Serial
439 dilution assay on different growth conditions at 30ºC of n=16 and n=3 isolates with either single
440 or duplicated rDNA. **c** Schematics of RNA-based assays in n=3 isolates with 1xrDNA vs 2xrDNA.
441 RTqPCR plots on three serial (1:10) dilutions of total RNA are used to estimate changes in the
442 amount of 18S and 25S ribosomal RNAs relative to the control messenger RNA, *TAF10*. **d**
443 Volcano plot showing RNA-seq data comparing transcriptomes of 1xrDNA and 2xrDNA strains
444 in triplicates. Red and blue dots indicate differentially expressed genes in 2xrDNA vs. 1xrDNA:
445 in blue downregulated in red upregulated ($P < 10{-}5$, |fold change| > 2).

446 **Figure 3 Stability of the rDNA locus is a function of chromosome position.**

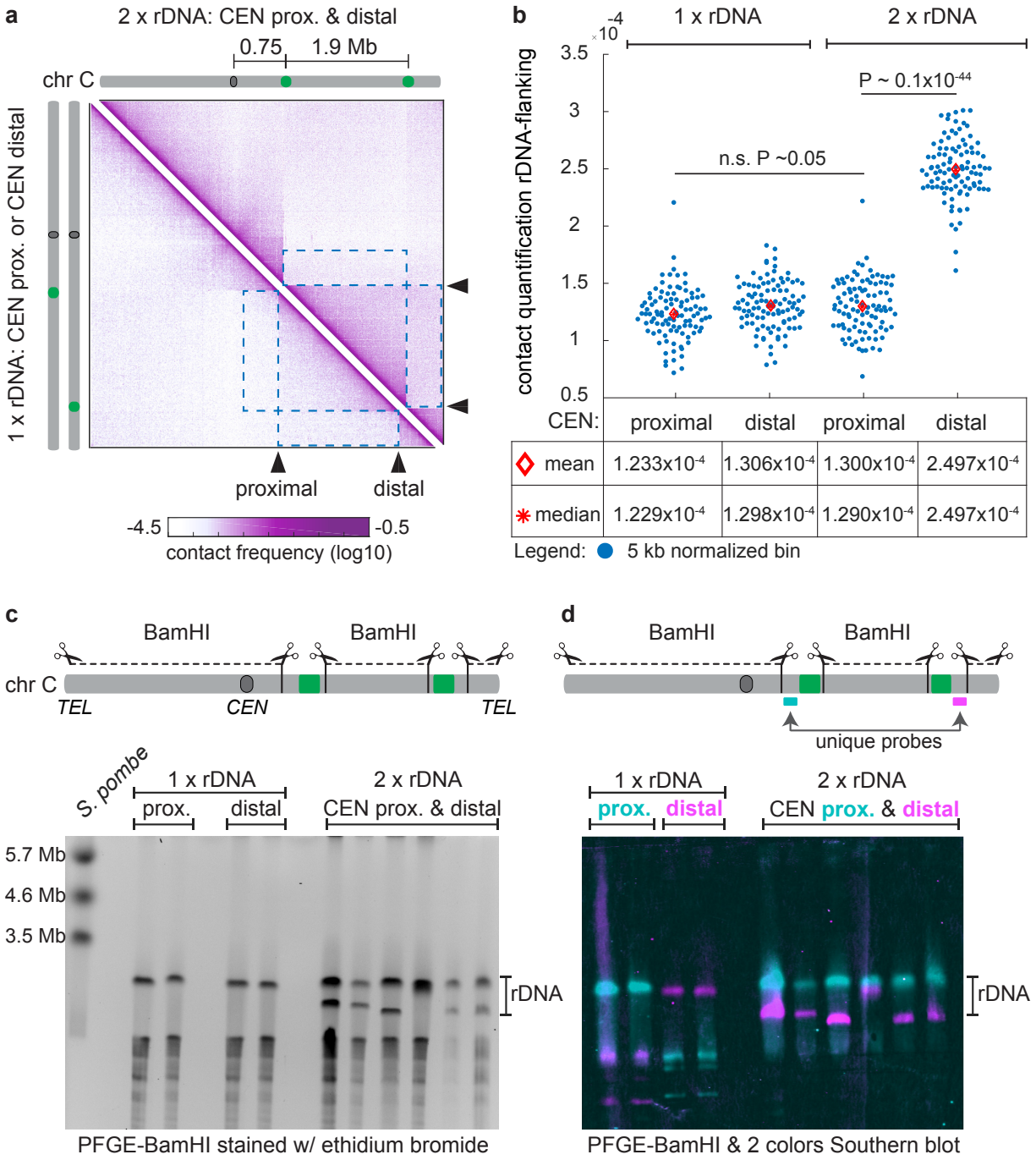

447

448 **Figure 3 Stability of the rDNA locus is a function of chromosome position.**

449 **a** Hi-C contact maps of megachromsome *C* (chr *C* in gray on the *x*- and *y*-axis of each contact
450 map) in *n*=3 strains with either one or two rDNA loci. Bottom left triangle map: average
451 representation of two merged contact maps with 1xrDNA per chr *C*, either *CEN* proximal or *CEN*
452 distal. Top right map: average representation of three merged contact maps with 2xrDNA per chr
453 *C*, *CEN* proximal and distal. rDNA distance from the centromere (dark gray) is indicated atop the
454 map. **b** Contact quantification between rDNA-flanking regions on chr *C*, highlighted in blue
455 rectangles in panel (a): 500 kb sequence, either upstream *CEN* proximal or downstream *CEN*
456 distal, and the 1.9 Mb sequence, downstream or upstream, respectively. Mean, median of absolute
457 contact values and their *P* values are indicated for each strain with either one or two rDNA loci. **c**
458 - **d** Estimate size of the rDNA arrays. PFGE of BamHI digested chromosomes (c) and the
459 corresponding Southern blot (d) with unique probes designed for each rDNA position. Schematic
460 indicates the position of rDNA arrays and probes (cyan or fuchsia) on chr *C*. PFGE run
461 specifications: *S. pombe* program for mega-size chromosome separation.

462 **Figure 4 Twin rDNA loci in *cis* form a single nucleolus during cell division.**

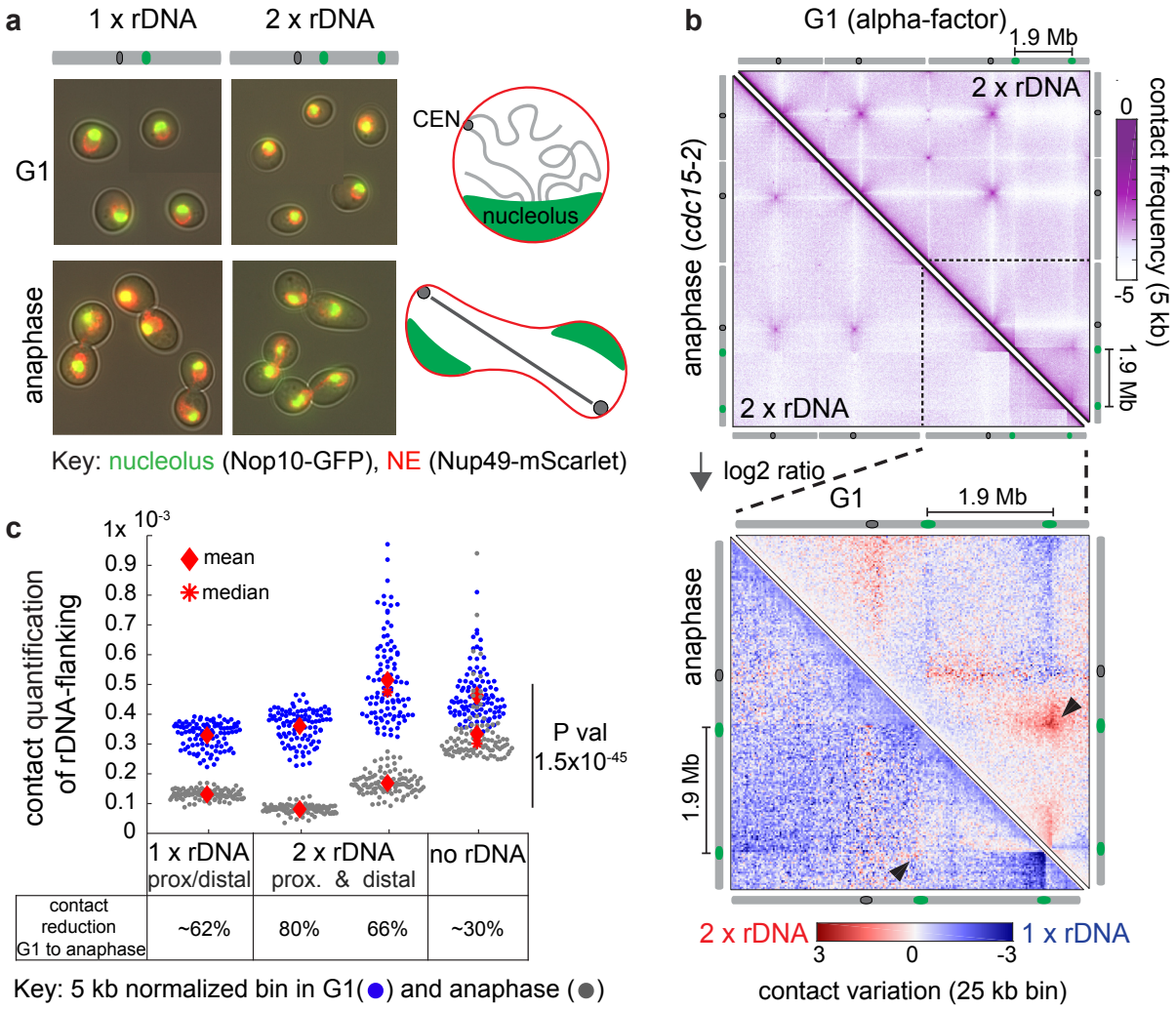

463

464 **Figure 4 Twin rDNA loci in *cis* form a single nucleolus during cell division.**

465 **a** Representative microscopy images of *n*=3 strains with one or two rDNA loci in *cis*. Cells were
466 synchronized in G1 (alpha-factor) and late anaphase (*cdc15-2* ts) before imaging. **b** Top panel: Hi-
467 C maps of megachromsomes in *n*=3, with two rDNA loci in *cis* on chr *C* (dashed outline), from
468 cells synchronized in G1 (top right map) and late anaphase (bottom left map). Bottom panel:
469 contact variation maps (log2-ratio) of chr *C* with 1xrDNA vs. 2xrDNA in G1 (top right map) vs.
470 late anaphase (bottom left map). Black arrowheads point at contact variations adjacent to the rDNA
471 loci. **c** Contact quantification between rDNA-flanking regions on chr *C*, as described in Figure 3b.
472 Relative percentages of contact reduction in anaphase compared to G1 are indicated for each strain
473 with one, two and no rDNA.

474 **Methods**

475 **Strains and culture conditions**

476 All strains used in this study are listed in Extended Data Table 1 and they are derived from BY4741
477 and BY4742[55] by transformation events. Deletion of the entire open reading frame of *SIR2* gene
478 was performed using the CRISPR-Cas9 with a single gRNA and a ~1 kb-long repair donor
479 generated by fusion PCR on *SIR2*-flanking sequences. The thermosensitive mutation in *CDC15*
480 (*cdc15-2* ts) was introduce with CRISPR-Cas9. Oligos used in this study are listed in Extended
481 Data Table 4.

482 Strains were grown in rich medium (YPD: 1% bacto peptone (Difco), 1% bacto yeast extract
483 (Difco) and 2% glucose; YPG: 1% bacto peptone (Difco), 1% bacto yeast extract (Difco) and 3%
484 glycerol) or in synthetic complete medium (SC: 0.67% yeast nitrogen base without amino acids
485 (Difco), supplemented with a mix of amino-acids and 2% glucose). Cells were grown at either
486 30°C or 24°C, the latter corresponds to the permissive temperature of the conditional
487 thermosensitive mutant *cdc15-2* (see also methods in Lazar-Stefanita et al., 2022 in press).

488 **Serial dilution assay and growth curves**

489 Yeast cultures from independent isolates of *n*=16 wild-type (WT) rDNA (BY4741), *n*=3 rDNA
490 *CEN* distal (JL411), *n*=3 rDNA *CEN* proximal (JL665) and *n*=3 rDNA *CEN* proximal and distal
491 (LS71) strains were grown in YPD liquid medium at 30ºC to saturation. For serial dilution assay:
492 yeast cultures in stationary phase were diluted to an optical density (OD) A_{600} = 0.1 and serially
493 diluted (1:10) in sterile water then spotted on different media (YPD, YPG and SC) and incubated
494 at different temperatures (30ºC and 37ºC) for 2 days. For growth curves: yeast cultures in
495 stationary phase were diluted in fresh YPD medium to A_{600} = 0.05, 200 µl were transferred to 96
496 well plates and every minute the BioTek Eon microplate spectrophotometer was programmed to

497 shake the plate and measure the A_{600} for a total of 24 h at 30ºC. A_{600} values were imported in
498 GraphPad Prism version 9 for Mac OS (GraphPad Software, San Diego, California USA,
499 www.graphpad.com) and used to calculate mean and standard deviation for each isolate of each
500 strain. Doubling time was calculated using the slope of the growth curves.

501 **rDNA Megablock engineering**

502 A CRISPR-Cas9 based method was used to promote during the cut-and-paste rDNA locus
503 relocation from the native location (flanked by chromosome 12 sequence) to an ectopic position
504 generated by fusing telomere 15R and telomere 4L. The method was performed as described by
505 Luo et al. *Nature* in 2018, except that two gRNAs cut the flanking regions of rDNA locus and the
506 third gRNA cuts at the new ectopic insertion site. In addition, three donor templates were generated
507 by fusion PCR, they include: (*i*) a donor template to rejoin the ends of the native locus upon rDNA
508 deletion, (*ii*) a donor template for bridging the left flanking region of the rDNA locus to its new
509 target location and (*iii*) a donor template for bridging the right flanking region of rDNA locus to
510 its new target location. rDNA translocation was verified by PCR with primer pairs designed
511 outside the newly formed chromosome junctions.

512 **Pulsed-field gel electrophoresis (PFGE) and Dual color Southern blot**

513 Chromosomes from stationary yeast cell cultures were prepared in agar molds using the Certified
514 Megabase Agarose (Bio-Rad CAT. 1613108) and pulsed-field gel electrophoresis (PFGE) was
515 carried out as previously described, with running conditions recommended for either *S. cerevisiae*
516 or *S. pombe* chromosomes. Specifically, megachromosomes were separated on a 0.8% agar gel in
517 1X TAE at 14ºC. Run time was ~72 h at 2V/cm with switch time of 20-30 min at an included angle
518 of 106º [16]. DNA size markers used were the *S. pombe* chromosomal DNA (Bio-Rad CAT. 170-
519 3633) and the *H. wingei* chromosomal DNA (Bio-Rad CAT. 170-3667).

520 Method for chromosome digestion: prior to the BamHI (NEB CAT. R0136L) incubation, agar
521 plugs were equilibrated 1X Buffer3.1 (NEB) for 24 h at 4ºC. BamHI digest was carried out for 24
522 h at 37ºC in ~500 µl final volume consisting of: ~100 mg agar, 50 µl 10X restriction buffer and 10
523 µl BamHI enzyme (200 U). Agar molds treated with BamHI were then used for the PFGE and
524 Southern blot.
525 The protocol for dual color Southern blot was optimized based on a previous study by Zavala et
526 al.[56]. Following electrophoresis of BamHI digested agar plugs, the gel was washed in: depurination
527 solution (0.25 M HCl) for 20 min, denaturation solution (0.5 M NaOH, 1.5 M NaCl) for 60 min
528 and neutralization solution (0.5 M Tris, 1.5 M NaCl pH 7.5) for 30 min. Chromosomes were
529 transferred by capillarity to a nylon membrane (Pall® 60208 Biodyne™ B Membrane, Pore Size
530 0.45 µm CAT. 60208) using 10X SSC buffer (20X SSC: 1.5 M NaCl, 0.3 M Sodium citrate pH 7)
531 for 72 h. After transfer the membrane was washed with 2X SSC for 5 min and baked at 80ºC for
532 30 min. Prehybridization and hybridization steps were performed at 50ºC in ULTRAhyb™
533 Ultrasensitive Hybridization Buffer (Invitrogen Ambion CAT. AM8670). PCR products (~1.1 kb-
534 long flanking unique sequences on either side of each rDNA locus) were labelled using Klenow
535 Fragment exo- (NEB CAT. M0212L) with either Biotin-16-dUTP (Roche CAT. 11093070910) or
536 Digoxigenin-11-dUTP alkali-stable (Roche CAT. 11093088910) at 37ºC for 1 h. Labelled DNA
537 probes were cleaned up using Zymo-Spin I Columns (Zymo Research CAT. C1003-50), denatured
538 at 95ºC for 5 min and ~300 ng of each were used for each hybridization experiment. The blot was
539 washed twice with 2X SSPE buffer (20X SSPE Buffer: 0.02 M EDTA and 2.98 M NaCl in 0.2 M
540 phosphate buffer pH 7.4; Sigma-Aldrich CAT. S2015) for 5 min at room temperature; twice with
541 2X SSPE, 1% SDS for 30 min at 55ºC; twice with 0.1X SSPE for 15 min at 55ºC. Blot was

542 incubated in Blocking buffer Odyssey (LI-COR® CAT. 927-40000) in 1X Tris-Buffered Saline
543 with 0.1% Tween 20 and 1% SDS for 3 h at room temperature.
544 The membrane was washed with 1X TBST for 5 min and incubated for 1 h at room temperature
545 with rabbit anti-DIG antibody (working concentration 1:2500 in Blocking buffer Odyssey;
546 ABfinity™ Rabbit Monoclonal, CAT. 700772). The primary antibody solution was washed out
547 three times with 1X TBST for 15 min at room temperature. The membrane was incubated in the
548 secondary antibody solution (working concentration 1:10000 in Blocking buffer Odyssey): Licor
549 IRDye® 800CW Streptavidin, 0.5 mg (CAT. 926-32230) and LIRDye® 680RD Goat anti-Rabbit
550 IgG (H + L), 0.5 mg (CAT. 926-68071) for 30 min at room temperature. Secondary antibody
551 solution was discarded and the membrane was washed three times with 1X TBST for 15 min at
552 room temperature before imaging acquisition using LI-COR Odyssey® Imager.

553 **Mating type switching**

554 Here we used the same reagents and protocol described by Zhang et al.[42].

555 **Sporulation and tetrad dissection**

556 A detailed protocol for mating, sporulation and tetrad dissection of yeast with fused chromosomes
557 was described by Luo et al.[16].

558 **RNA extractions**

559 Total RNA was extracted from 3 independent isolates of *n*=16 WT rDNA (BY4741), *n*=3 rDNA
560 *CEN* distal (JL411), *n*=3 rDNA *CEN* proximal (JL665) and *n*=3 rDNA *CEN* proximal and distal
561 (LS71) strains. Approximately $2x10^8$ cells were harvested from log phase cultures (1.5-2 $x10^7$
562 cells/ml) grown in YPD medium at 30ºC. Cell pellets were washed in RNase free water and
563 resuspended in RNA lysis buffer (50 mM Tris-HCl pH 8, 100 mM NaCl). Cells were lysed
564 mechanically using acid-washed glass beads (Sigma-Aldrich CAT. G8772-100G) at 4ºC. The

565 RNA was extracted by phenol:chloroform:isoamylalcohol (ThermoFisherScientific CAT. 15593)
566 and ethanol precipitated. Extractions were treated with DNaseI (Agilent CAT. 600031) for 1 h at
567 37ºC and RNA quality was verified by agarose gel in 1X TAE.

568 **RT-qPCR**

569 The above total RNA extractions were serial diluted (1:10/100/1000) and used for RT-qPCR
570 reactions with gene specific oligos (18S, 25S and TAF10). The reverse transcriptase (RT) reaction
571 was performed according to the manufacturer protocol SuperScript™ IV Reverse Transcriptase
572 (Invitrogen CAT. 18090050). Successively, quantitative PCR was performed using the
573 LightCycler® 480 SYBR Green I Master (Roche CAT. 04887352001) and the standard
574 amplification protocol with 45 cycles in a multi-well PCR plate 384. Ct values for each replicate
575 were imported in GraphPad Prism version 9 for Mac OS (GraphPad Software, San Diego,
576 California USA, www.graphpad.com) and used to calculate mean and standard deviation for each
577 gene in each strain. The three plots generated, that correspond to each gene, show Ct variation in
578 function of the RNA dilution factor and strain.

579 **RNA library preparation, sequencing and analysis**

580 Stranded total RNA-seq libraries were prepared with the QIAseq stranded RNA library kit
581 (Qiagen, CAT. 180743) following the manufacture's recommendations using dual indexing
582 primers. Additionally, the input total RNA was first processed with the QIAseq FastSelect rRNA
583 Yeast kit to remove cytoplasmic and mitochondrial rRNA (Qiagen, CAT. 334215). Library quality
584 was assessed using the ZAG 110 dsDNA kit on (Agilent, CAT. ZAG-110-5000) and run on the
585 ZAG DNA analyzer system (Agilent). Libraries were then sequenced on an Illumina NextSeq 500
586 using the 75-cycle high output in paired end mode (Illumina, CAT. 20024906).

587 Differential gene analysis (Extended Data Table 2). RNA sequencing analysis was performed as
588 previously described[57] using kallisto/sleuth suite with minor modifications. Briefly, reads were
589 processed by Illumina barcode and quality trimming with Trimmomatic[58] and quality assessed
590 with FastQC. Next, reads were aligned using the pseudo-alignment program kallisto[59] to the
591 reference S288C genome[60], with annotations supplied with a gtf file containing all annotated
592 RNAs in stranded paired end mode (options, --genomebam --gtf --fr-stranded). The output of
593 kallisto was then used for data analysis in sleuth[61]. Volcano plots were generated using the Walds
594 test false discovery rate adjusted *P* value ($p<0.01$) and log2 fold change (-2>Log2FC>2).

595 **Cell cycle synchronization**

596 For both imaging and Hi-C experiments yeast cells, carrying either a single rDNA locus (LS88,
597 LS95) or two rDNA loci in *cis* (LS90, LS103), were synchronized in either G1 with alpha-factor
598 (Zymo Research, CAT. Y1001), or in late anaphase, using the thermosensitive mutant *cdc15-2*.
599 Method for G1 synchronization (LS88 and LS90): cells were grown to saturation in 5 ml SC
600 medium at 30ºC, the next day cells were subcultured in 150 ml fresh SC medium (optical density,
601 OD, A_{600}=0.5) for 2 h 30 min at 30ºC then alpha-factor was added (final concentration: 25 μM)
602 and cultures were incubated for additional 2 h 30 min at 24ºC before imaging and formaldehyde
603 crosslink.
604 Method for late anaphase synchronization (LS95 and LS103): cells were grown to saturation in 5
605 ml SC medium at 24ºC, the next day they were subcultured in 150 ml fresh SC medium (A_{600}=0.5)
606 and grown for 5 h at 24ºC then the temperature was switched to 37ºC (non-permissive condition)
607 and incubated for additional 3 h before imaging and formaldehyde crosslink.
608 The quality of G1 and anaphase synchronizations was visually monitored by microscopy hourly.
609 For microscopy small aliquots (~1-2 ml synchronized cultures) were spooned down at 3000g for

610 3 min and fixed in ethanol 70%; whereas, the remaining cultures were fixed with formaldehyde
611 for Hi-C library preparation (see below).

612 **Protein tagging and imaging of the nucleolus**

613 The cell cycle reorganization of the nucleolus within the nucleus was monitored using
614 fluorescently tagged proteins at their endogenous C-terminus. Nuclear envelope was labelled with
615 either mCherry (*NIC96::mCherry*) or mScarlet (*NUP49::mScarlet*), while the nucleolus with GFP
616 (*NOP10::EGFP*) as described by Zhang et al.[42] (see also strain genotype in Extended Data Table
617 1). Imaging was performed on the EVOS M7000 microscope using the Olympus X-APO 100 Oil,
618 1.45NA/WD 0.13mm (Oil) objective. Images were acquired as Z-stacks and visualized as max
619 intensity projections using ImageJ[62].

620 **Hi-C library preparation and data analysis**

621 Hi-C libraries (Extended Data Table 3) were prepared from yeast cells harvested from either log
622 phase or cell cycle synchronized cultures (see above protocols for cell synchronizations). Methods
623 for yeast Hi-C library preparation and data analysis were performed as previously described by
624 Lazar-Stefanita et al., 2017; 2022. Briefly, Hi-C reads were aligned using Bowtie 2[63] and processed
625 using command lines based on HiCLib tool developed in the Mirny lab (Imakaev et al., 2012).
626 Normalized contact maps (Sequential Component Normalization)[64] were 5 kb-binned and were
627 plotted using MatLab R2018 (The MathWorks, Inc., Natick, Massachusetts, United States).

628 The Hi-C assay resulted crucial to validate the transplantation of the rDNA locus. We found that
629 among the potential candidates - that were PCR positive for the rDNA transplantation - only one
630 isolate had the entire locus relocated that resulted in the actual re-positioning of the rDNA
631 boundary from the native location (centromere-distal: 2.75 Mb from the active centromeric
632 sequence, *CEN15,* and 0.6 Mb from the nearest telomeric sequence, *TEL12R*) to the new ectopic

633 position at the fusion junction between the left arm of former chromosome *15* and the right arm of
634 former chromosome *4* (centromere-proximal: 0.75 Mb from *CEN15* and 2.52 Mb from *TEL12R*).
635 Of note, in the isolates that were false positives by PCR for the rDNA megablock transplantation,
636 the chromosome boundary formed by this locus remained at the original location (centromere-
637 distal) as expected.
638 The Hi-C maps were used to evaluate the strength of each rDNA boundary in function of their
639 distance from the centromere and locus number (single vs. double) across megachromosome *C*.
640 For this analysis we firstly reasoned that the chromosome boundaries observed at the location of
641 the rDNA loci on the 2D maps are 'visual artifacts' due to the combination of different structural
642 characteristics at this locus. Indeed, the highly repetitive nature and the formation of a subnuclear
643 compartment (nucleolus) appear to lower the contact frequency between the rDNA-flanking
644 regions. Along the same lines we also expected that differences in structure and/or size between
645 rDNA loci would have an effect on the strength of the correspondent chromosome boundaries. In
646 other words, bigger the rDNA locus ('bulkier' the nucleolus) lower the contact frequency between
647 its flanking sequences, therefore stronger the boundary. To compare between the *CEN* proximal
648 and *CEN* distal rDNA boundaries, located in single or double copy on megachromosome *C*, we
649 used normalized maps (5 kb-binned) to quantify contacts between 500 kb-long regions (flanking
650 either the right or the left end of each locus) and the 1.9 Mb region upstream/downstream or
651 enclosed by two loci (see highlighted regions in blue on chr *C* maps in Figure 3a). Spread point
652 plots, where each point corresponds to total contacts made by each 5 kb bin, were generated for
653 each rDNA boundary using Matlab. *P* values were calculated using the Kolmogorov–Smirnov test
654 (K–S test) function in MATLAB 2018a (The MathWorks, Inc., Natick, Massachusetts, United
655 States).

656 Log2 ratios of Hi-C contact maps were used for their pairwise comparison and the contact
657 probability decay in function of the genomic distance, $p(s)$, was computed to assess the status of
658 the chromatin fiber. Both these analyses were performed as previously described by Lazar-
659 Stefanita et al., 2017; 2022 in press.

Acknowledgments

We acknowledge all members of Boeke lab for their assistance. We thank Aleksandra Wudzinska and Gregory W. Goldberg for their assistance and helpful comments on the manuscript. This work was supported by National Science Foundation grants MCB-1616111 and MCB-1921641 and NIH grant RM1HG009491 to JDB.

Author Contributions

LLS and JDB designed the research project. LLS performed the experiments with help from: JL that relocated the rDNA array, WZ that built *n*=16 with rDNA on heterologous chromosomes and MH that performed and analyzed RNAseq. LLS wrote the manuscript and all authors contributed to editing.

Additional Information

Genome-wide and RNA sequencing files were deposited at the NCBI database as FASTQ files. See BioProject accession number PRJNA847233 for the SRA data. The reviewer link: https://dataview.ncbi.nlm.nih.gov/object/PRJNA847233?reviewer=6h4lqpu2o2epg0f4ta40dlmqo4

Competing interests

Jef Boeke is a Founder and Director of CDI Labs, Inc., a Founder of Neochromosome, Inc, a Founder of and Consultant to ReOpen Diagnostics, and serves or served on the Scientific Advisory Board of the following: Modern Meadow, Inc., Rome Therapeutics, Inc., Sample6, Inc., Sangamo, Inc., Tessera Therapeutics, inc., and the Wyss Institute. The remaining authors declare no competing interests.

Extended Data Tables and Figures

Title:

Stable twin rDNA loci form a single nucleolus in brewer's yeast

Authors

Luciana Lazar-Stefanita[1], Jingchuan Luo[1†], Max A. B. Haase[1,2], Weimin Zhang[1], Jef D. Boeke[1,3]*

*, Corresponding author: jef.boeke@nyulangone.org

Affiliations

[1] Institute for Systems Genetics and Department of Biochemistry and Molecular Pharmacology, NYU Langone Health, New York, NY 10016, USA

[2] Vilcek Institute of Graduate Biomedical Sciences at NYU School of Medicine

[3] Department of Biomedical Engineering, NYU Tandon School of Engineering, Brooklyn NY 11201 USA

† Present address: Whitehead Institute for Biomedical Research, Cambridge, MA, 02142, USA

Extended Data Tables:

Extended Data Table 1 List of strains used in this study.

Extended Data Table 2 RNA seq. list of differentially expressed genes.

Extended Data Table 3 Hi-C libraries.

Extended Data Table 4 List of primers used in this study.

Extended Data Figures and Figure Legends:

Extended Data Figure 1 rDNA locus transplantation and duplication at ectopic chromosomal locations.

Extended Data Figure 2 Effects of rDNA duplication on genome stability and cell fitness.

Extended Data Figure 3 Stability of the rDNA locus in function of chromosome position and silencing.

Extended Data Figure 4 Cell cycle reorganization of the chromosome with twin rDNA loci in *cis*.

Extended Data Figure 5 Duplicated rDNA loci may lead to chromosome mispairing in meiosis.

31 **Extended Data Tables**

Strain name	Parent	Genotype	No. Chr.	rDNA location	Ref.
BY4741	S288C	*MAT**a** his3Δ1 leu2Δ0 met15Δ0 ura3Δ0*	16	Chr *12*	(Brachmann et al., 1998)
WZ456	BY4742	*MAT**a** his3Δ1 leu2Δ0 lys2Δ0 ura3Δ0 rdn::C-S.ITS-LEU2 NOP10::EGFP-KanMX, NIC96::mCherry-HIS3*	16	Chr *12*	(Zhang et al., 2017)
WZ457	BY4742	*MAT**a** his3Δ1 leu2Δ0 lys2Δ0 ura3Δ0 rdn::NatMX4 NOP10::EGFP-KanMX, NIC96::mCherry-HIS3 YCR018C / C-S.ITS-LEU2 / YCR019W*	16	Chr *3*	(Zhang et al., 2017)
WZ499	Spore of yWZ456 X yWZ457	*MAT**a** his3Δ1 leu2Δ0 lys2Δ0 ura3Δ0 rdn::C-S.ITS-LEU2 NOP10::EGFP-KanMX, NIC96::mCherry-HIS3, YCR018C / C-S.ITS-LEU2 / YCR019W*	16	Chr *12* + Chr *3*	(Zhang et al., 2017)
JL411	BY4741	*MAT**a** his3Δ1 leu2Δ0 met15Δ0 ura3Δ0*	3	Chr *C* distal	(Luo et al., 2018a)
JL665	JL411	*MAT**a** his3Δ1 leu2Δ0 met15Δ0 ura3Δ0*	3	Chr *C* proximal	This work
LS88	JL665	*MAT**a** his3Δ1 leu2Δ0 met15Δ0 ura3Δ0 NOP10::EGFP-KanMX NUP49::mScarlet-S.p.HIS5*	3	Chr *C* proximal	This work
LS95	LS88	*MAT**a** his3Δ1 leu2Δ0 met15Δ0 ura3Δ0 cdc15-2(Ts) NOP10::EGFP-KanMX NUP49::mScarlet-S.p.HIS5*	3	Chr *C* proximal	This work
LS70	JL665 X JL411	*MAT**a/alpha** his3Δ1/ his3Δ1 leu2Δ0/ leu2Δ0 met15Δ0/met15Δ0 ura3Δ0/ura3Δ0*	3	Chr *C* proximal & Chr *C* distal	This work
LS71-C1&C2	Spore of LS70	*MAT**alpha** his3Δ1 leu2Δ0 met15Δ 0ura3Δ0*	3	Chr *C* proximal + distal	This work
LS71-C3	Spore of LS70	*MAT**a** his3Δ1 leu2Δ0 met15Δ0 ura3Δ0*	3	Chr *C* proximal + distal	This work
LS90	LS71-C3	*MAT**a** his3Δ1 leu2Δ0 met15Δ0 ura3Δ0 NOP10::EGFP-KanMX NUP49::mScarlet-S.p.HIS5*	3	Chr *C* proximal + distal	This work
LS91	Haploids of JL411	*MAT**a/alpha** his3Δ1/ his3Δ1 leu2Δ0/ leu2Δ0 met15Δ0/met15Δ0 ura3Δ0/ura3Δ0*	3	Chr *C* distal & Chr *C* distal	This work

LS92	Haploids of JL665	*MAT**a/alpha** his3Δ1/ his3Δ1 leu2Δ0/ leu2Δ0 met15Δ0/met15Δ0 ura3Δ0/ura3Δ0*	3	Chr *C* proximal & Chr *C* proximal	This work
LS93	LS71-C1 X LS71-C3	*MAT**a/alpha** his3Δ1/ his3Δ1 leu2Δ0/ leu2Δ0 met15Δ0/met15Δ0 ura3Δ0/ura3Δ0*	3	Chr *C* proximal + distal & Chr *C* proximal + distal	This work
LS103	LS90	*MAT**a** his3Δ1 leu2Δ0 met15Δ0 ura3Δ0 cdc15-2(Ts) NOP10::EGFP-KanMX NUP49::mScarlet-S.p.HIS5*	3	Chr *C* proximal & distal	This work
LS130 (LS131)	JL411	*MAT**a** his3Δ1 leu2Δ0 met15Δ0 ura3Δ0 sir2Δ*	3	Chr *C* distal	This work
LS141 (LS142)	Diploid (*SIR2/ sir2Δ*)	*MAT**a** or **alpha** his3Δ1 leu2Δ0 met15Δ0 ura3Δ0 sir2Δ*	3	Chr *C* proximal & distal	This work
LS143 (LS144)	Diploid (*sir2Δ/ sir2Δ*)	*MAT**a** or **alpha** his3Δ1 leu2Δ0 met15Δ0 ura3Δ0 sir2Δ*	3	Chr *C* proximal & distal	This work

Extended Data Table 1 List of strains used in this study.

Extended Data Table 2 RNA seq. list of differentially expressed genes.

Data presented as excel spreadsheet file.

37

Strain name	Karyotype (*n*, #rDNA-position)	Synchronization method	Total paired-end reads	Aligned paired-end reads	Total contacts in 5 kb-binned maps
JL411	3, 1-distal	none	24770805	19642950	5273769
JL665	3, 1-proximal	none	24447393	19581599	3662044
LS70	3, 1-distal + 1-prox	none	34383730	27174746	4918384
LS71-C1	3, 1-distal + 1-prox	none	29910065	20997502	3292606
LS71-C2	3, 1-distal + 1-prox	none	26807590	18886934	3585706
LS71-C3	3, 1-distal + 1-prox	none	32026043	23014301	4020070
LS88	3, 1-proximal	G1	12605198	8902009	5362318
LS90	3, 1-distal + 1-prox	G1	8820734	5893335	4041830
LS95	3, 1-proximal	Anaphase *cdc15-2*	12933900	9479614	6106239
LS103-C1	3, 1-distal + 1-prox	Anaphase *cdc15-2*	15026254	10109053	3904083
LS103-C2	3, 1-distal + 1-prox	Anaphase *cdc15-2*	28339485	20719596	4170357

38 **Extended Data Table 3 Hi-C libraries.** For each library it reports: number of chromosomes per
39 strain (*n*), number of rDNA per chromosome, synchronization method and total Hi-C contacts.
40

41 **Extended Data Table 4 List of primers used in this study.**

42 Data presented as excel spreadsheet file.

43 **Extended Data Figure 1 rDNA locus transplantation and duplication at ectopic chromosomal**

44 **locations.**

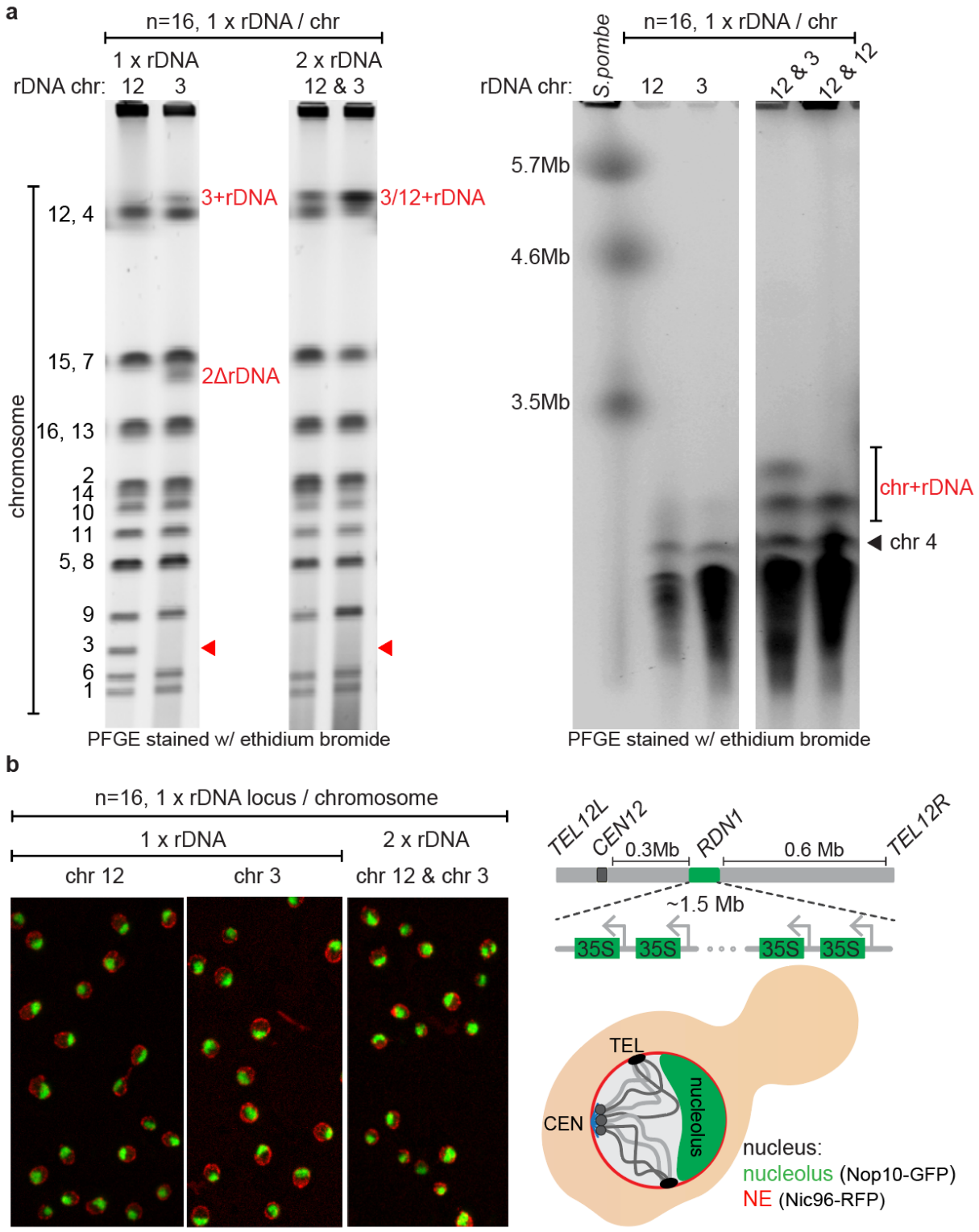

45

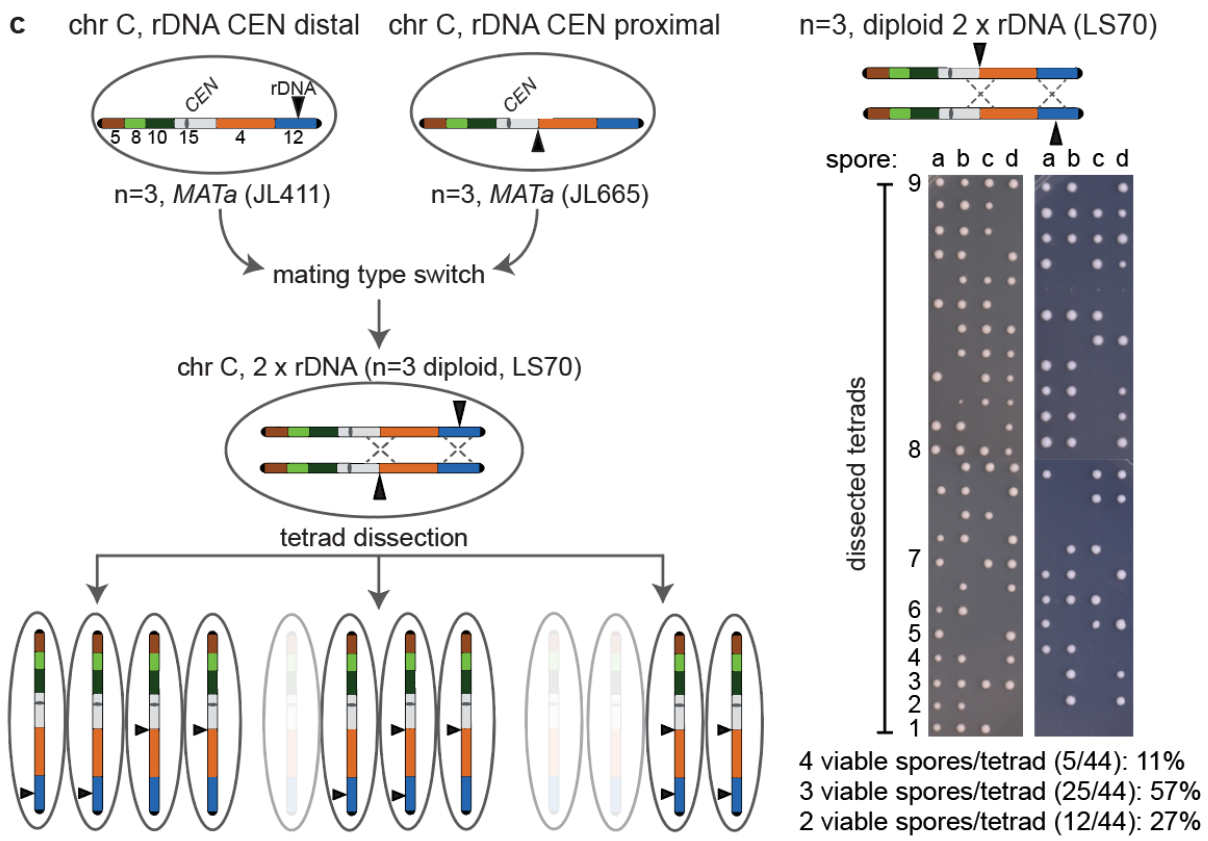
c
chr C, rDNA CEN distal
chr C, rDNA CEN proximal
n=3, diploid 2 x rDNA (LS70)
CEN
rDNA
5 8 10 15 4 12
n=3, MATa (JL411)
n=3, MATa (JL665)
mating type switch
chr C, 2 x rDNA (n=3 diploid, LS70)
tetrad dissection
spore: a b c d a b c d
dissected tetrads
9
8
7
6
5
4
3
2
1
4 viable spores/tetrad (5/44): 11%
3 viable spores/tetrad (25/44): 57%
2 viable spores/tetrad (12/44): 27%

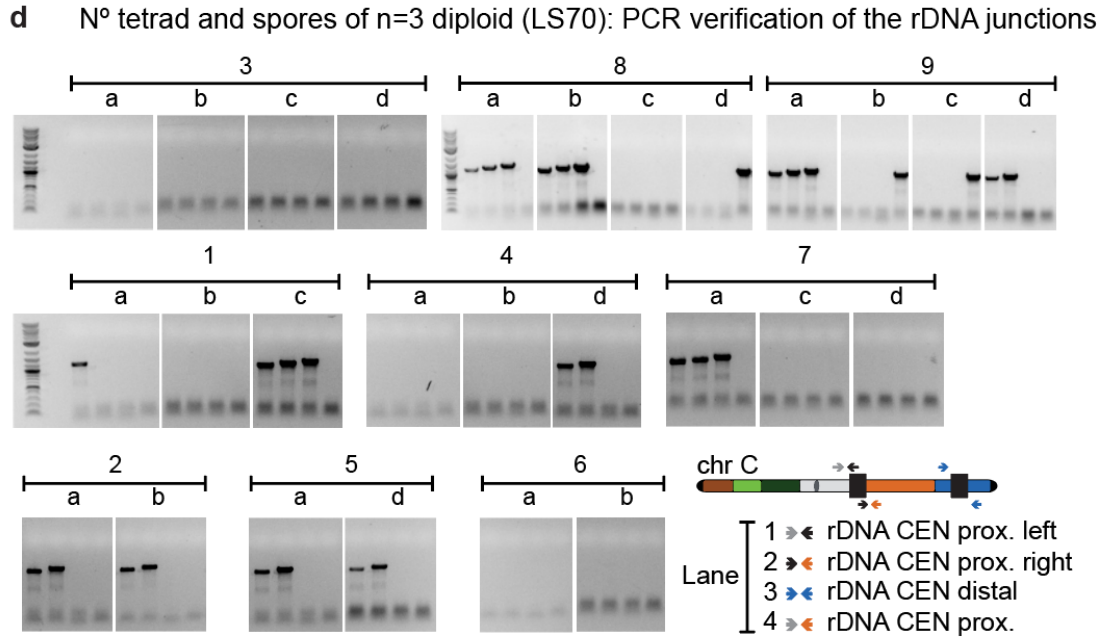
d
Nº tetrad and spores of n=3 diploid (LS70): PCR verification of the rDNA junctions
3
a b c d
8
a b c d
9
a b c d
1
a b c
4
a b d
7
a c d
2
a b
5
a d
6
a b
chr C
Lane
1 rDNA CEN prox. left
2 rDNA CEN prox. right
3 rDNA CEN distal
4 rDNA CEN prox.

47 **Extended Data Figure 1 rDNA locus transplantation and duplication at ectopic chromosomal**
48 **locations.**

49 **a** Chromosome separation by PFGE of wild-type yeasts with 16 chromosomes (*n*=16) with single
50 or two rDNA loci on different chromosomes (red indicates chromosomes that have lost or gain the
51 rDNA locus). Two distinct programs are used for chromosome separation: *S. cerevisiae* on the left
52 and *S. pombe* on the right. **b** Representative microscopy images of yeast nuclei with single or two
53 rDNA loci as described in Figure 1a, b. **c** Diagram showing the strategy used to duplicate the
54 rDNA locus within the same arm of megachromosome *C* in *n*=3 (chr *C* is colorcoded according to
55 the chromosome fusion design). Right panels show spores of individual tetrads (asci) of *n*=3
56 diploid with two rDNA loci in asymmetric *trans* locations. **d** Verification of rDNA duplication by
57 junction PCR, sampling 4 different sequences in 27 spores originated from 9 different tetrads.
58 Positive spores for rDNA duplication show PCR products in lane 1 and 2 only.

59 **Extended Data Figure 2 Effects of rDNA duplication on genome stability and cell fitness.**

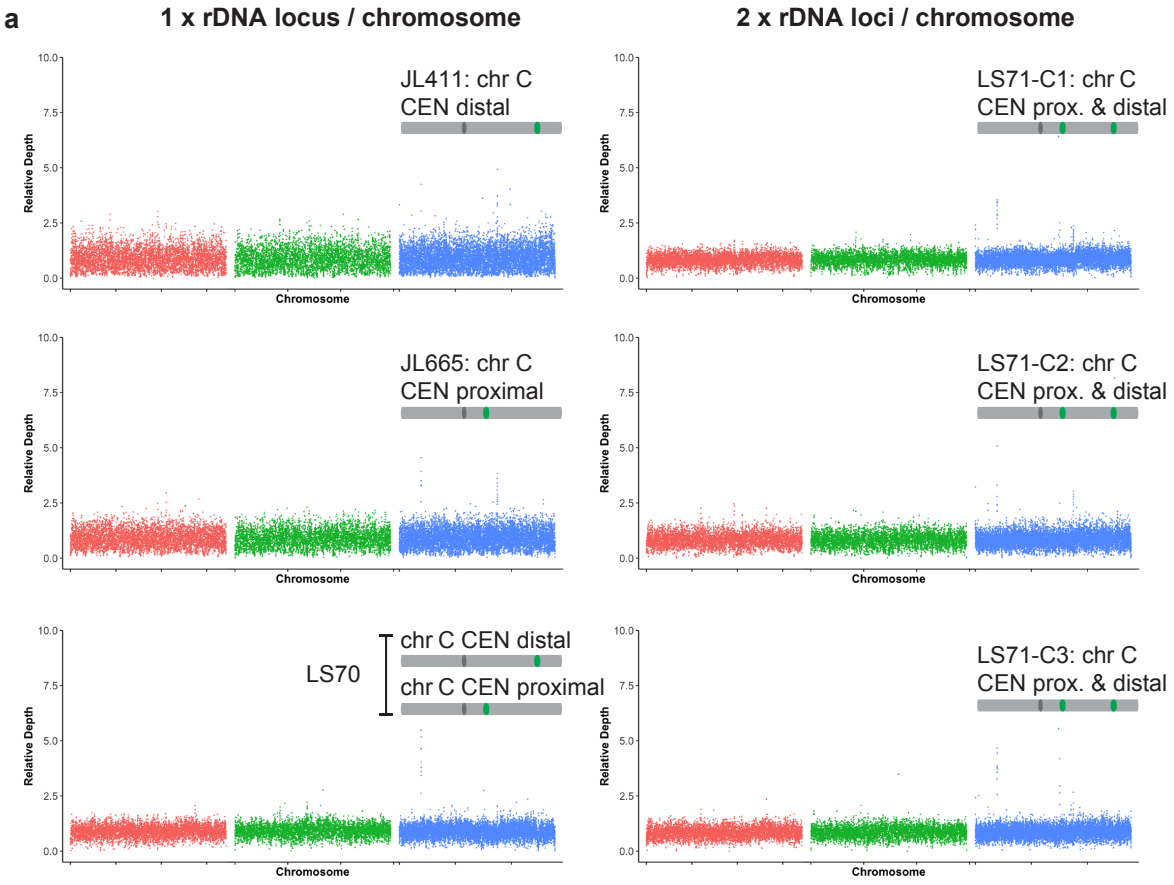

60

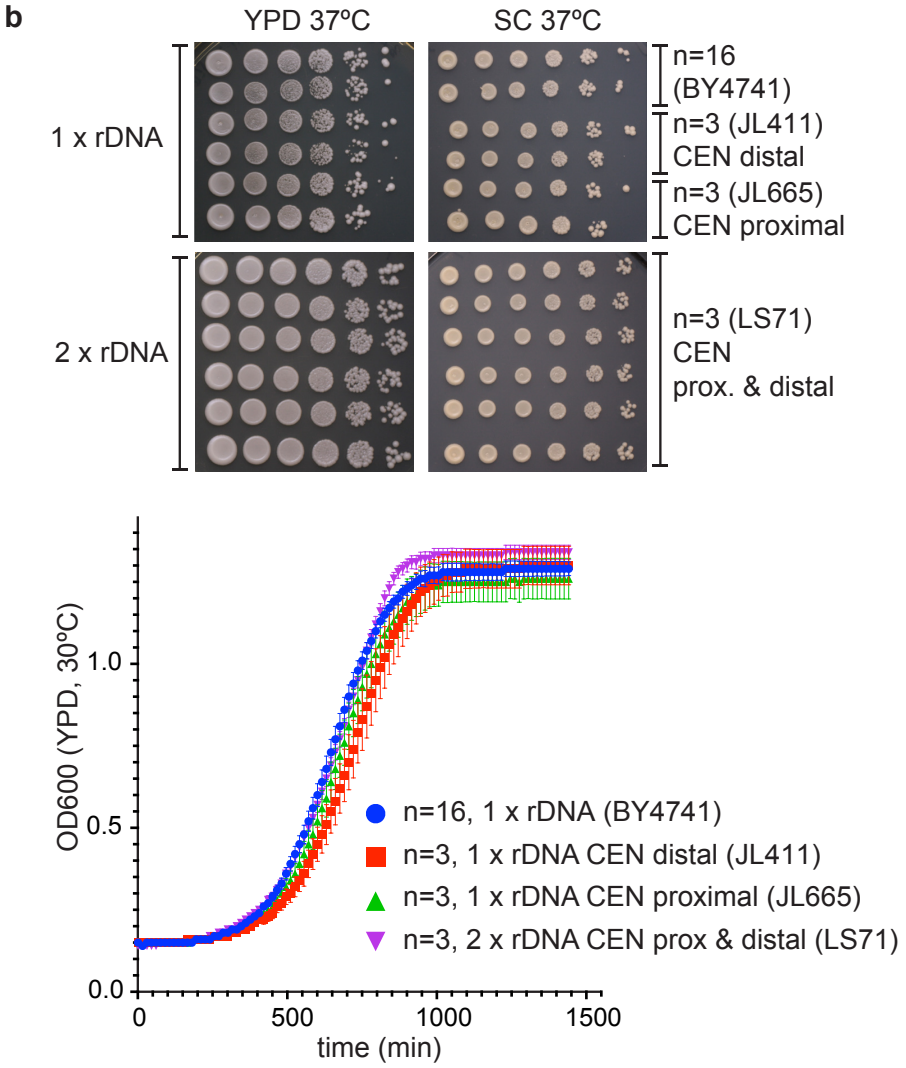
b
YPD 37ºC
SC 37ºC
1 x rDNA
2 x rDNA
n=16
(BY4741)
n=3 (JL411)
CEN distal
n=3 (JL665)
CEN proximal
n=3 (LS71)
CEN
prox. & distal
OD600 (YPD, 30ºC)
0.0
0.5
1.0
0
500
1000
1500
time (min)
n=16, 1 x rDNA (BY4741)
n=3, 1 x rDNA CEN distal (JL411)
n=3, 1 x rDNA CEN proximal (JL665)
n=3, 2 x rDNA CEN prox & distal (LS71)

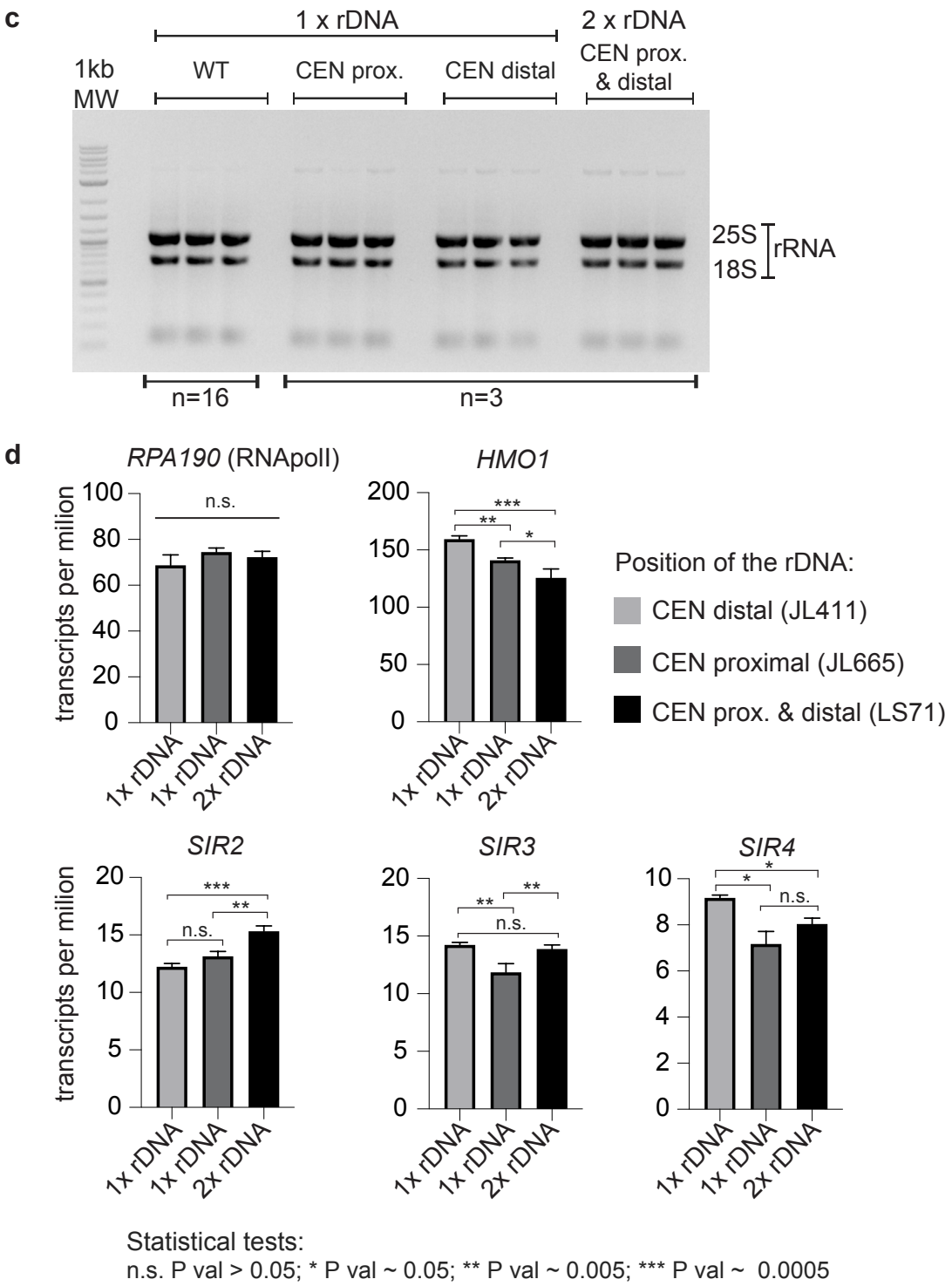
c
1 x rDNA
2 x rDNA
1kb MW
WT
CEN prox.
CEN distal
CEN prox. & distal
25S
18S
rRNA
n=16
n=3
d
RPA190 (RNApolI)
HMO1
SIR2
SIR3
SIR4
transcripts per milion
n.s.
1x rDNA
2x rDNA
Position of the rDNA:
CEN distal (JL411)
CEN proximal (JL665)
CEN prox. & distal (LS71)
Statistical tests:
n.s. P val > 0.05; * P val ~ 0.05; ** P val ~ 0.005; *** P val ~ 0.0005

63 **Extended Data Figure 2 Effects of rDNA duplication on genome stability and cell fitness.**

64 **a** Relative genome sequencing depth plots (ggplot2 function in R) of *n*=3 strains with a single
65 rDNA locus on chr *C* (haploids: JL411 and JL665 with either *CEN* distal or *CEN* proximal locus,
66 respectively; diploid: LS70 with *CEN* distal and proximal) or two loci on chr *C* (independent
67 haploids: LS71 C1 to C3). Sequencing depth for each megachromosome is colorcoded differently;
68 chr *C* is displayed on the top right of each plot. **b** Fitness assays of *n*=16 and *n*=3 isolates. Top
69 panels: serial dilution assays on different growing conditions at 37ºC see also Figure 2b. Bottom
70 panel: growth curves reporting optical densities (OD^{A600}) in YPD at 30ºC. **c** Agarose gel reporting
71 the quality of the total RNA extracted from *n*=16 and *n*=3 isolates with different rDNA number
72 and position relative to Figure 2c. **d** Bar plots showing transcriptional changes of a specific subset
73 of genes (mainly involved in the metabolism of ribosomal DNA and RNA) in *n*=3 with a different
74 number and position of the rDNA locus see also Figure 2d.

75 **Extended Data Figure 3 Stability of the rDNA locus in function of chromosome position and**

76 **silencing.**

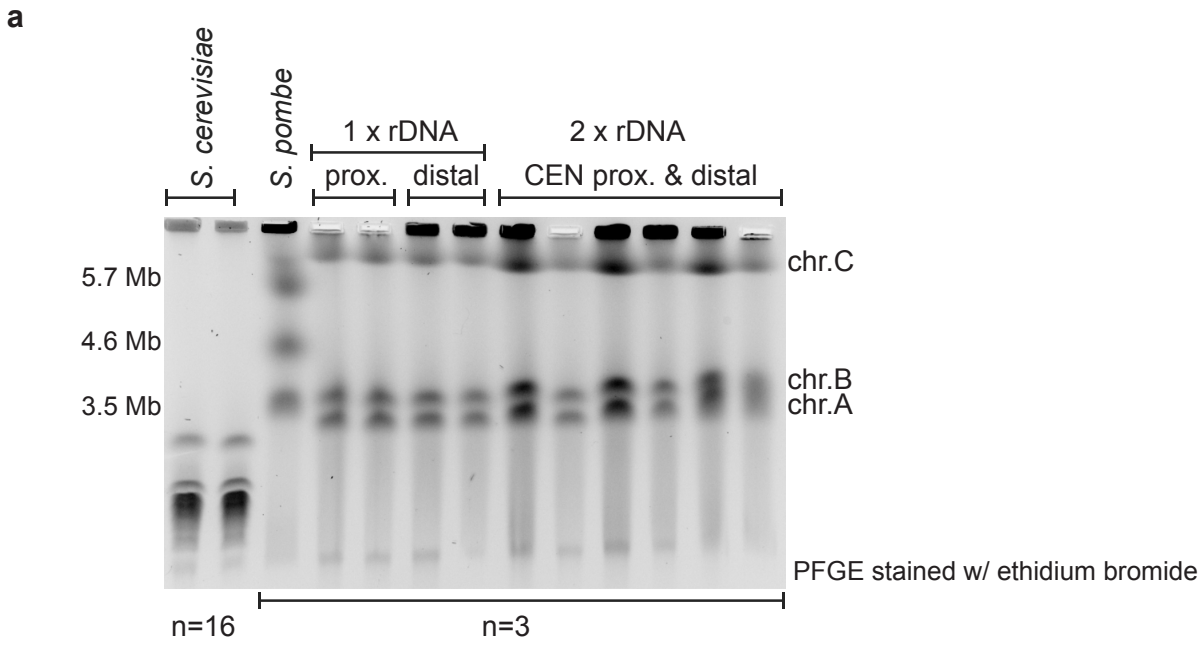

77

b

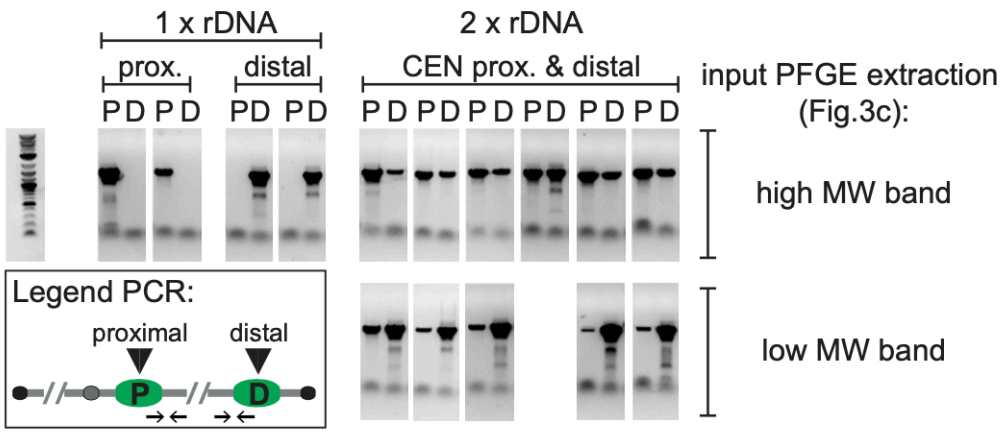

c

1. Evolution experiment:

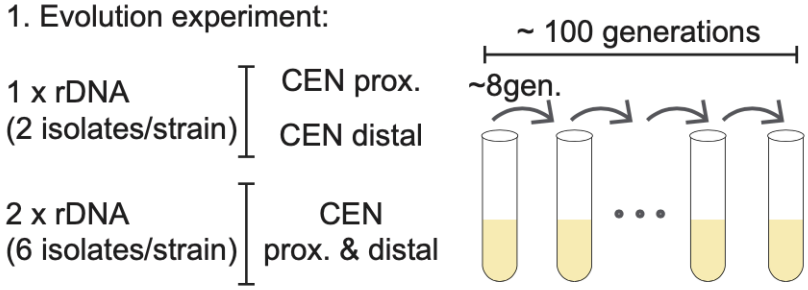

2. PFGE + BamHI digest after propagating for 100 generations:

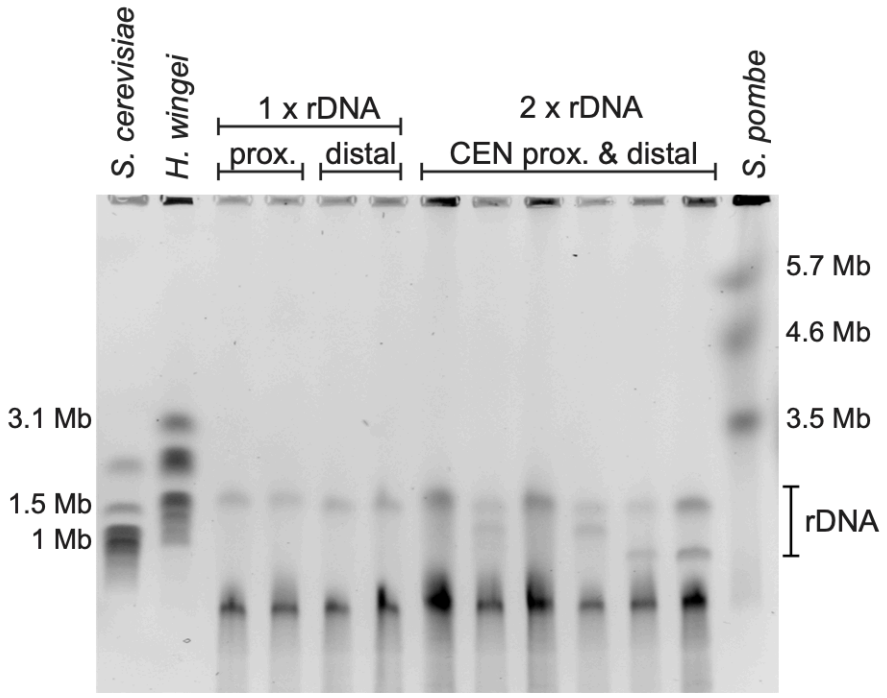

PFGE-BamHI stained w/ ethidium bromide

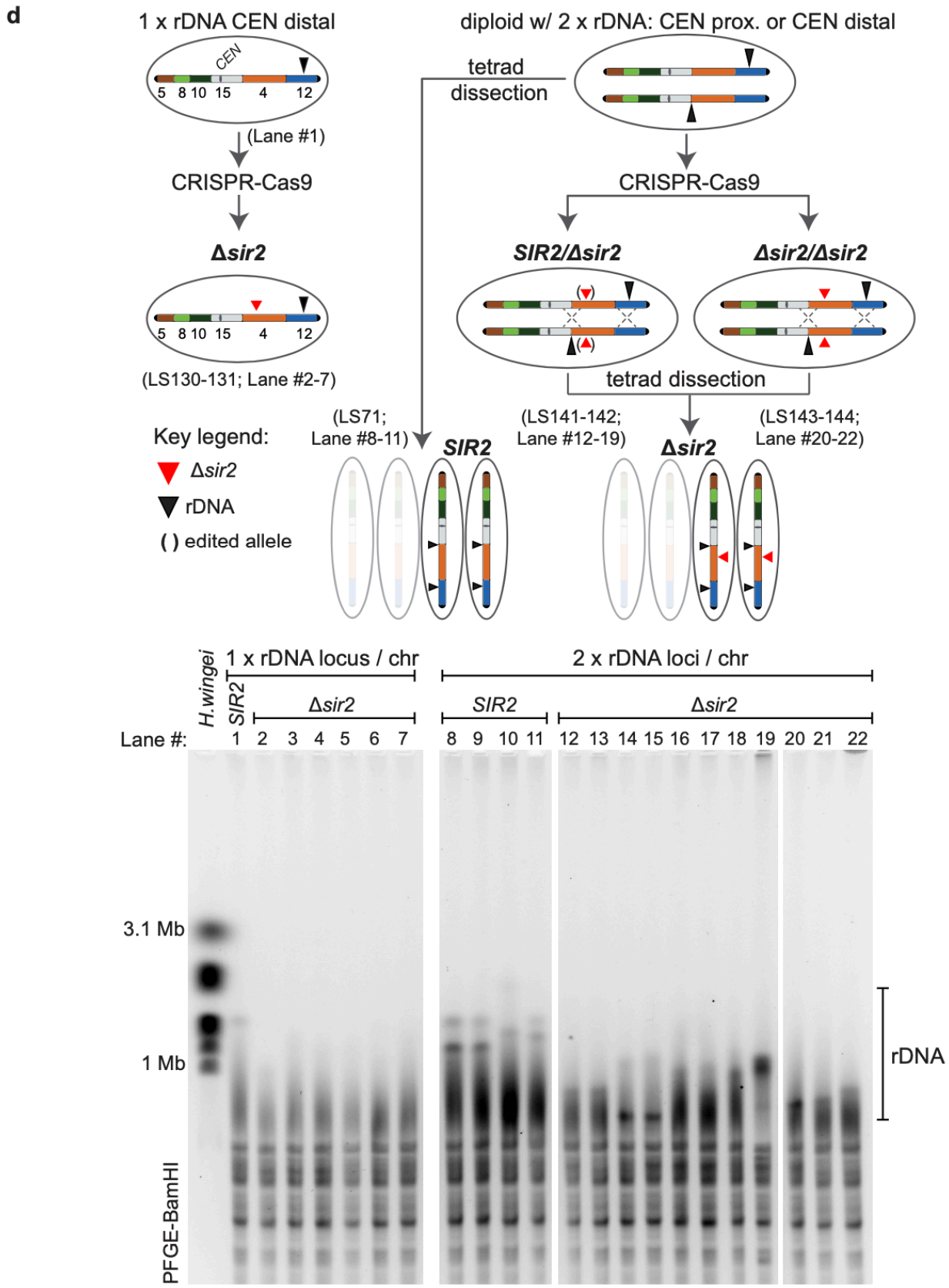
d
1 x rDNA CEN distal
CEN
5 8 10 15 4 12
(Lane #1)
CRISPR-Cas9
Δsir2
5 8 10 15 4 12
(LS130-131; Lane #2-7)
diploid w/ 2 x rDNA: CEN prox. or CEN distal
tetrad dissection
CRISPR-Cas9
SIR2/Δsir2
Δsir2/Δsir2
tetrad dissection
(LS71; Lane #8-11)
(LS141-142; Lane #12-19)
(LS143-144; Lane #20-22)
SIR2
Δsir2
Key legend:
Δsir2
rDNA
( ) edited allele
H.wingei
SIR2
1 x rDNA locus / chr
2 x rDNA loci / chr
Δsir2
SIR2
Δsir2
Lane #:
1 2 3 4 5 6 7
8 9 10 11
12 13 14 15 16 17 18 19 20 21 22
3.1 Mb
1 Mb
PFGE-BamHI
rDNA

80 **Extended Data Figure 3 Stability of the rDNA locus in function of chromosome position and**
81 **silencing.**
82 **a** Chromosome separation by PFGE of different isolates of *n*=16 and *n*=3 strains, with either one
83 or two rDNA loci. PFGE run specifications: *S. pombe* program for mega-size chromosome
84 separation. **b** PCR-validations of rDNA proximal (P) and distal (D) junctions. DNA template
85 extracted from PFGE, rDNA bands that migrated at high or low molecular weights in Figure 3c. **c**
86 Schematics of the evolution experiment in *n*=3 strains with a different number and position of the
87 rDNA locus. Cell populations from different isolates were evolved long-term (~100 generations)
88 in batch cultures and used to assess the size of the rDNA arrays using PFGE and BamHI digest.
89 PFGE program as described in panel (a). **d** Diagram of the approach used to assess rDNA array
90 stability in function of Sir2. CRISPR-Cas9 was used to delete *SIR2* gene in *n*=3 haploid with one
91 rDNA locus, and in the diploid with two rDNA loci in *trans* and asymmetric. Haploid spores with
92 two *cis* rDNA loci obtained from sporulation of different diploids (*SIR2/SIR2, SIR2/sir2, sir2/sir2*)
93 were used to assess stability of the rDNA arrays by PFGE and BamHI digest. PFGE program as
94 described in panel (a).

95 **Extended Data Figure 4 Cell cycle reorganization of the chromosome with twin rDNA loci**

96 **in *cis*.**

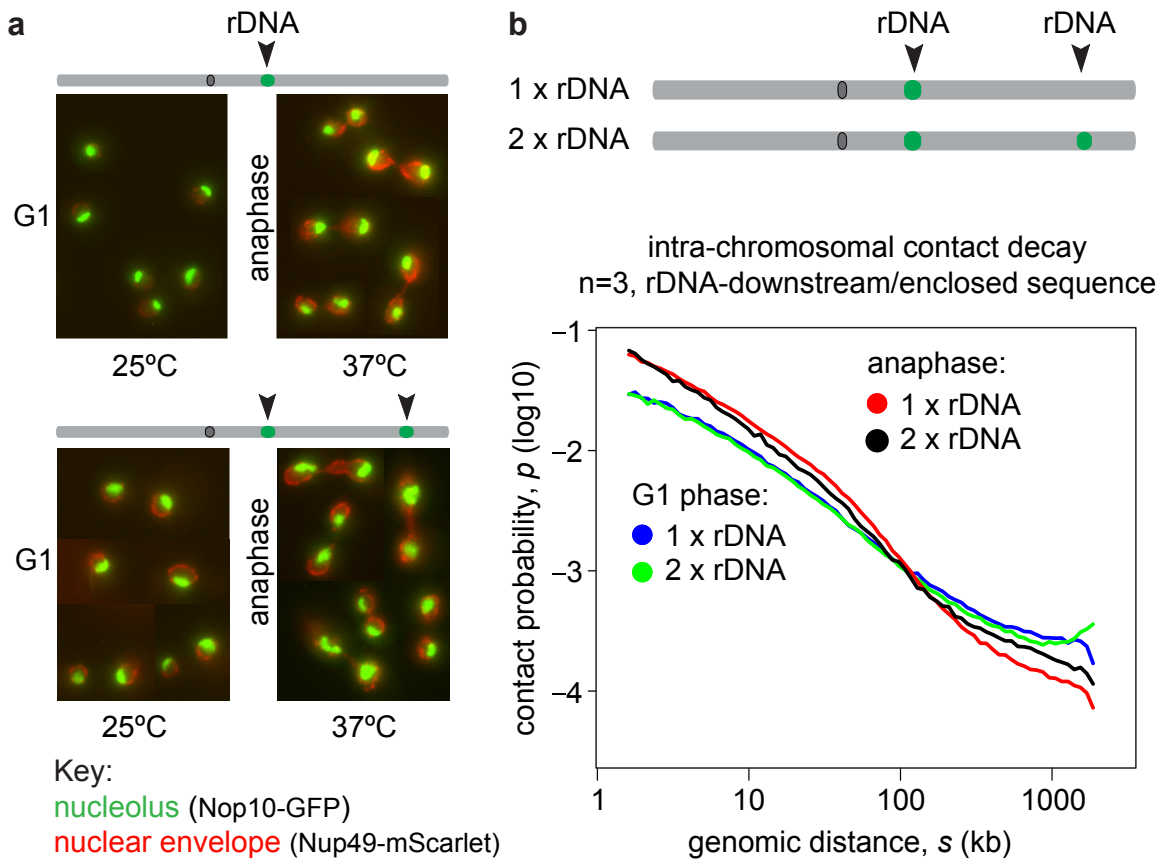

97

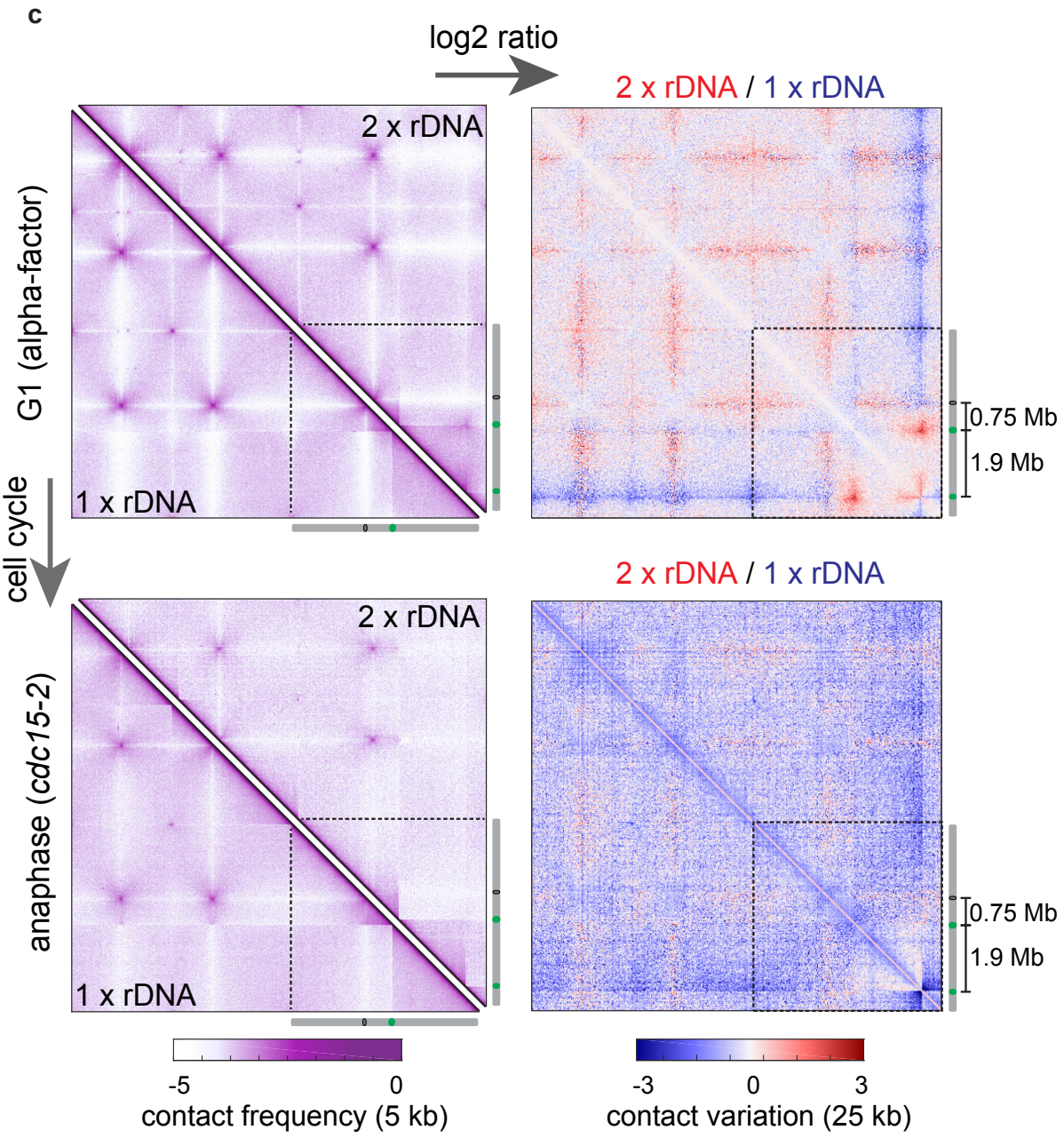
c
log2 ratio
2 x rDNA / 1 x rDNA
2 x rDNA
1 x rDNA
G1 (alpha-factor)
cell cycle
anaphase (cdc15-2)
0.75 Mb
1.9 Mb
-5
0
contact frequency (5 kb)
-3
0
3
contact variation (25 kb)

Extended Data Figure 4 Cell cycle reorganization of the chromosome with twin rDNA loci in *cis*.

a Representative microscopy images of *n*=3 nuclei, with one or two rDNA loci, in cells synchronized in G1 (alpha-factor, growth at 25ºC) and late anaphase (*cdc15-2* ts, growth at 37ºC). **b** Contact probability decay *p*(*s*) in G1 vs. anaphase: shows the average decay of the intrachromosomal contact frequency p between loci with respect to their genomic distance *s*. **c** Left panels: Hi-C maps of megachromosomes in *n*=3, with one or two rDNA on chr *C* (dashed outline), from cells synchronized in G1 (top triangle maps) and late anaphase (bottom triangle maps). Right panels: contact variation (log2-ratio) of the maps shown on the left (G1: top square map and anaphase: bottom square map).

Extended Data Figure 5 Duplicated rDNA loci may lead to chromosome mispairing in meiosis.

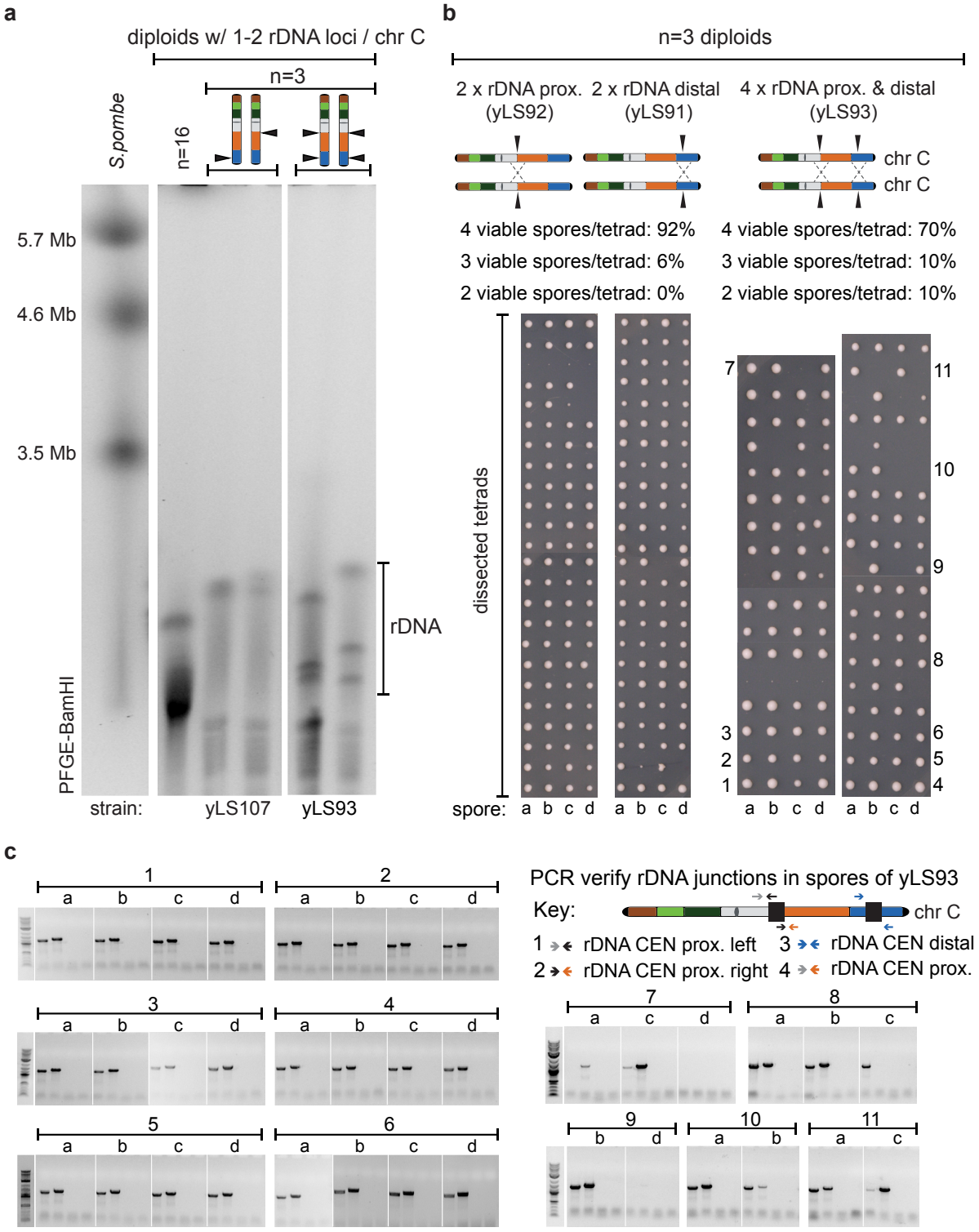

111

112 **Extended Data Figure 5 Duplicated rDNA loci may lead to chromosome mispairing in**
113 **meiosis.**
114 **a** PFGE and BamHI digest of diploids of *n*=16 and *n*=3 strains, with different number and position
115 of the rDNA locus. Run specifications: *S. pombe* program for mega-size chromosome separation.
116 **b** Sporulation experiments of *n*=3 diploids with single and double pairs of rDNA loci. Percentage
117 of tetrads (asci) with 2, 3 or 4 viable spores is indicated for each strain. **c** PCR verification of rDNA
118 junctions, sampling 4 different sequences in 36 spores originated from 11 different tetrads.